Joint Beamforming and Power Allocation for M2M/H2H Co-Existence in Green Dynamic TDD Networks: Low-Complexity Optimal Designs

Chi-Han Lee, *Student Member, IEEE*, Ronald Y. Chang, *Senior Member, IEEE*, Shin-Ming Cheng, *Member, IEEE*, Chia-Hsiang Lin, *Member, IEEE*, and Chiu-Han Hsiao, *Member, IEEE*

***Abstract*—Coexistence and interference management issues for machine-to-machine (M2M) and human-to-human (H2H) communications are crucial for the Internet of Things (IoT). This article considers beamforming and power allocation for M2M/H2H coexistence networks adopting the dynamic time division duplex (TDD) spectrum sharing scheme and energy harvesting (EH). The design objective is total system power minimization with device Quality-of-Service (QoS) constraints as well as EH constraints. Since the dynamic TDD introduces new types of interference, i.e., uplink/downlink cross-interference, the considered problem is a challenging nonconvex coupled problem. We first consider a simplified problem without the EH considerations. We propose a novel low-complexity algorithm based on uplink-downlink duality (UDD) and alternating optimization (AO) to tackle this problem. Then, we propose a second-order cone programming (SOCP) relaxation-based AO low-complexity algorithm to deal with the general problem. In the simulation, we study the performance of the QoS, the number of antennas, the number of users, and the power splitting ratio. Finally, the performance of the proposed algorithms have low-complexity than the classical convex optimization method.**

***Index Terms*—Beamforming, dynamic time-division duplex (TDD), energy harvesting (EH), Internet of Things (IoT), machine-type communication (MTC).**

Manuscript received February 5, 2021; revised July 12, 2021; accepted August 19, 2021. Date of publication September 2, 2021; date of current version March 7, 2022. This work was supported in part by the Ministry of Science and Technology (MOST), Taiwan, under Grant MOST 106-2628-E-001-001-MY3, Grant MOST 109-2221-E-001-013-MY3, Grant MOST 108-2628-E-011-007-MY3, and Grant MOST 109-2923-E-011-006-MY3; in part by the Einstein Program (Young Scholar Fellowship Program) of MOST under Grant MOST 110-2636-E-006-026; and in part by the Higher Education Sprout Project of Ministry of Education (MOE) to the Headquarters of University Advancement at National Cheng Kung University (NCKU). This article was presented in part at the IEEE International Conference on Communications (ICC), Dublin, Ireland, June 7–11, 2020. *(Corresponding authors: Ronald Y. Chang; Chia-Hsiang Lin.)*

Chi-Han Lee and Shin-Ming Cheng are with the Department of Computer Science and Information Engineering, National Taiwan University of Science and Technology, Taipei 106, Taiwan, and also with the Research Center for Information Technology Innovation, Academia Sinica, Taipei 115, Taiwan (e-mail: d10202006@mail.ntust.edu.tw; smcheng@mail.ntust.edu.tw).

Ronald Y. Chang and Chiu-Han Hsiao are with the Research Center for Information Technology Innovation, Academia Sinica, Taipei 115, Taiwan (e-mail: rchang@citi.sinica.edu.tw; chiuhanhsiao@citi.sinica.edu.tw).

Chia-Hsiang Lin is with the Department of Electrical Engineering and the Miin Wu School of Computing, National Cheng Kung University, Tainan 70101, Taiwan (e-mail: chiahsiang.steven.lin@gmail.com).

Digital Object Identifier 10.1109/JIOT.2021.3109697

I. Introduction

In FUTURE communication applications, such as the Internet of Things (IoT) [2], [3], industry 4.0, 5G, and 6G, massive machine-type devices (MTDs) and human-type devices (HTDs) coexistence issues are an emerging network architecture [4]–[10]. MTDs, such as robot vacuum cleaner, healthcare sensor, and security monitor, have potential applications in smart industries (industry 4.0), smart cities, driverless cars, etc. HTDs are characteristic people interface in cellular networks and communication standards, i.e., smartphones and tablets. In general, MTD and HTD are also named as machine-to-machine (M2M) and human-to-human (H2H) in most literature, respectively, [1], [5]. Although NB-IoT and LTE-M have been proposed by 3rd Generation Partnership Project (3GPP) standardization [3], [11] to specify low-power and narrowband M2M, the simultaneous wireless information and power transfer (SWIPT)/energy harvesting (EH) technology has been attracted for the IoT field [12]–[20]. In [15], a robust beamforming method has been investigated to deal with the imperfect successive information cancellation and channel uncertainty during channel state information in IoT. In [16], the SWIPT is considered to assist ultrareliable low latency communication with finite blocklength codes in IoT networks. In [17], Dinkelbach and bisection method are using to deal with the energy efficiency SWIPT optimization problem for IoT. Based on the cognitive radio IoT network, [18] uses the beamforming method for secure communication. To energy sustainable IoT, [19] has studied SWIPT multicasting in a downlink (DL) multiple-input single-output (MISO) scenario. In [20], K-means and weighted minimum mean square error (MMSE) methods have been proposed to deal with the weighted sum-rate maximization problem for massive connectivity IoT. The above literature mainly researches the EH IoT or IoT while not cope with the M2M/H2H coexistence issue in the IoT field. Although [21] consider EH HTDs/MTDs coexistence issue, authors just deal with the uplink (UL) case without DL scenario and transceiver beamforming design.

In order to deal with dense small cells in 5G and enable their efficient operations, 3GPP has introduced a flexible time division duplex (TDD) scheme which is termed the *dynamic TDD* [22]–[25]. Dynamic TDD [24]–[32] is a spectrum usage scheme that flexibly adjusts DL and UL transmission in a

TDD fashion by utilizing the traffic asymmetry between DL and UL. There are two advantages of dynamic TDD. First, dynamic adjustment UL and DL are suitable for ultradense network (UDN) due to real-time asynchronous multimedia communications. Second, sharing the spectrum of the adjacent cells is effective as network slicing [24]. Dynamic TDD however introduces new types of interference, i.e., UL-to-DL and DL-to-UL cross-link interference, when UL transmission is performed in one cell and DL transmission in a neighbor cell, concurrently. Recently, different application of research literature in dynamic TDD has a single cell [26], two cells [1], [25], [27], [28], and multicell [29]–[32]. In a single cell dynamic TDD scenario [26], device-to-device mode selection and transmission time allocation have been investigated. In two cells dynamic TDD scenario, macrocell-aided femtocell and interference management have been studied in [25], [27], and [28]. Considering multicell dynamic TDD, the beamforming technique is using to deal with cross-link interference [29]–[32]. However, to the best of our knowledge, considering dynamic TDD as a spectrum usage scheme for M2M/H2H EH coexistence networks has not been totally examined in the literature.

Our contributions in this article, which is different from the previous literatures, are summarized as follows.

1) To the best of our knowledge, this is the first paper to study joint beamforming and power allocation (JBPA) design for the coexistence, resource allocation, and interference management issues in green dynamic TDD networks enabled IoT. Previous works considering static (conventional) TDD cannot accommodate uneven UL and DL traffic demands across different adjacent cells, which often arise in IoT scenarios. In addition, we propose the EH (a.k.a. SWIPT) in dynamic TDD to deal with cross-link interference. The augmented EH constraints further pose some challenges in the optimization algorithm design and analysis, for the latter we achieved rank-one solution guarantees as illustrated next (see also Theorems 1 and 4).
2) We consider two related problems in the framework of green dynamic TDD networks, with solutions of own merit for each problem. We first address a simplified problem assuming no EH capabilities at each device. In this optimization problem, we formulate the power minimization in the objective function under per-HTD/MTD Quality-of-Service (QoS) constraints via transmit power allocation in the UL network and transceiver beamforming in UL/DL networks. We propose a novel uplink-downlink duality (UDD)-based algorithm, and compare it with prior arts of semidefinite relaxation (SDR) and second-order cone program (SOCP) methods. We show that the SDR solution satisfies the rank-one constraint, and, therefore, does not lose optimality as a result of rank relaxation in this dynamic TDD networks problem. As demonstrated analytically and numerically, the proposed UDD method has much lower computational complexity than SDR and SOCP without loss any system performance. This design method is suitable applied for the upcoming 6G and IoT area with conceivable massive numbers of machines, antennas, and devices.
3) We address the general problem where each IoT device possesses EH capabilities. The structural properties of the additional EH requirement constraint and power-splitting (PS) ratio constraint render the UDD-based algorithm for the simplified problem not applicable to the general problem. We propose an SOCP relaxation-based algorithm to solve the general problem based on a series of SOCP relaxation procedures. Numerical results demonstrate that the proposed method has the same optimal value as the EH constraint SDR method, with lower computational complexity.

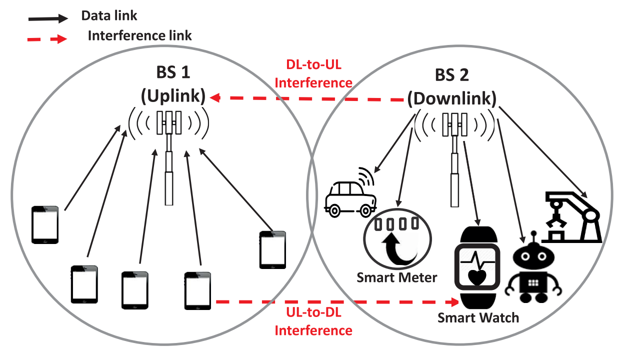

Fig. 1. According to 3GPP, in two cell dynamic TDD system, this article considers a scenario wherein BS 1 (resp., BS 2) serves UL HTDs (resp., DL MTDs) using a dynamic UL/DL resource management scheme.

The remainder of this article is organized as follows. Section II describes the MTD/HTD coexistence network with dynamic TDD spectrum sharing and EH. Section III presents the problem formulation with and without EH capabilities. Sections IV and V present approaches to solve the problem without and with EH, respectively. Numerical results and discussions are presented in Section VI. Finally, we discuss the conclusions and future work in Section VII.

Notations: Throughout this article, we denote that matrices and vectors are denoted by the bold uppercase and lowercase letters, respectively. The superscripts $(\cdot)^M$ and $(\cdot)^H$, respectively, express MTD and HTD. Transpose and Hermitian transpose denote $(\cdot)^\top$ and $(\cdot)^\dagger$, respectively. The real and imaginary parts denote $\mathrm{Re}(\cdot)$ and $\mathrm{Im}(\cdot)$, respectively. The trace of a matrix and the complex space matrices are denoted as $\mathrm{Tr}(\cdot)$ and $\mathbb{C}^{m\times n}$, respectively.

II. System Model

Consider a two-cell dynamic TDD network with or without EH, in which one cell handles UL HTDs, while the other cell serves DL MTDs, as depicted in Fig. 1. This should be commonly seen in future daily life [1], [8]. For example, consider a smart factory in industry 4.0 or an unmanned store, built in a residential area, where the factory/store is full of MTDs, while, outside the factory, there are just some typical HTDs in the residential area. Dynamic TDD is an adaptive adjustment of the TDD UL/DL time slot in an adjacent cell. For example, in dynamic TDD two cell mechanism, it admits UL or DL communication at the same time in two cells (as in traditional TDD mechanism), as well as UL in one cell and DL in an adjacent cell (as depicted in Fig. 1, and is a main focus of this article). Fig. 1 plots an exemplary dynamic TDD operation scenario where one cell serves HTDs in the UL while the other cell serves MTDs in the DL, similar to [1], [8], and [27]. Reversed UL/DL directions in the two cells, i.e., one cell serves HTDs in the DL while the other cell serves MTDs in the UL, can be readily accommodated in the framework of this work due to symmetry. There are K MTDs in the DL network and L HTDs in the UL network. The DL BS has N_t^{D} antennas, the UL BS has N_r^{U} antennas, and each HTD/MTD has a single antenna. Let $\mathcal{L} = \{1, \ldots, L\}$ and $\mathcal{K} = \{1, \ldots, K\}$ be the index set of HTDs and MTDs, respectively. Each device has EH capabilities. For the scenario shown in Fig. 1, each MTD can receive information as well as harvest energy from the serving BS. Therefore, in the DL cell (BS 2 in Fig. 1), the system is a well-known MISO SWIPT scenario.

In the DL transmission, $\sum_{k=1}^{K} \boldsymbol{w}_k s_k^{\mathrm{M}}$ is the transmitted signal from the DL BS. $s_k^{\mathrm{M}} \in \mathbb{C}$ is a zero mean, unit-variance signal destined for the kth MTD, and $\boldsymbol{w}_k \in \mathbb{C}^{N_t^D \times 1}$ is the associated beamforming vector. The received signal at the kth ($k \in \mathcal{K}$) MTD is given by

$$y_k^{\mathrm{M}} = \underbrace{\boldsymbol{h}_k^{\dagger}\boldsymbol{w}_k s_k^{\mathrm{M}}}_{\substack{\text{desired}\\ \text{signal}}} + \underbrace{\boldsymbol{h}_k^{\dagger}\sum_{i\neq k}^{K}\boldsymbol{w}_i s_i^{\mathrm{M}}}_{\substack{\text{intracell}\\ \text{interference}}} + \underbrace{\sum_{\ell=1}^{L} h_{k,\ell}\sqrt{p_\ell^{\mathrm{H}}} s_\ell^{\mathrm{H}}}_{\substack{\text{UL-to-DL}\\ \text{interference}}} + \underbrace{n_k^{\mathrm{M}}}_{\text{noise}} \quad (1)$$

where the channel from the DL BS to the kth MTD is denoted by $\boldsymbol{h}_k \in \mathbb{C}^{N_t^D \times 1}$, the channel from the transmitter of the ℓth UL HTD to the kth DL MTD is denoted by $h_{k,\ell}$, p_ℓ^{H} and s_ℓ^{H} are the transmit power and transmit signal of the ℓth UL HTD, respectively, and n_k^{M} is the additive white Gaussian noise (AWGN) with distribution $\mathcal{CN}(0, (\sigma_k^{\mathrm{M}})^2)$.

Each MTD adopts a PS-based EH scheme. In the information decoding (ID) component, the PS factor is ρ_k ($0 \leq \rho \leq 1$) at the kth MTD. In the EH component, the PS factor is $1 - \rho_k$ at the kth MTD. The received signal at the ID of the kth MTD is

$$\widetilde{y}_k^{\mathrm{M}} = \sqrt{\rho_k} y_k^{\mathrm{M}} + \widetilde{n}_k^{\mathrm{M}}, \ k \in \mathcal{K} \quad (2)$$

where $\widetilde{n}_k^M$ is the AWGN introduced by the ID in the decoding process with distribution $\mathcal{CN}(0, \widetilde{\sigma}_k^2)$. The distribution of $\widetilde{n}_k^M$ is independent of n_k^M. The signal-to-interference-plus-noise ratio (SINR) at the kth MTD is given by

$$\mathrm{SINR}_k^M = \frac{\rho_k |\boldsymbol{h}_k^{\dagger}\boldsymbol{w}_k|^2}{\rho_k\left(\sum_{i\neq k}^{K} |\boldsymbol{h}_k^{\dagger}\boldsymbol{w}_i|^2 + \sum_{\ell=1}^{L} |h_{k,\ell}|^2 p_\ell^H + (\sigma_k^{\mathrm{M}})^2\right) + \widetilde{\sigma}_k^2}. \quad (3)$$

The harvested energy that can be stored by the kth MTD is given by

$$y_k^{\mathrm{EH}} = \xi_k^M (1 - \rho_k)\left(\sum_{i=1}^{K} |\boldsymbol{h}_k^{\dagger}\boldsymbol{w}_i|^2 + \sum_{\ell=1}^{L} |h_{k,\ell}|^2 p_\ell^H + (\sigma_k^{\mathrm{M}})^2\right) \quad (4)$$

where $\xi_k^M \in (0, 1]$ is the energy conversion efficiency of the EH circuits at the kth MTD.

In the UL transmission, the received signal at the BS from all HTDs is given by

$$\boldsymbol{y}^{\mathrm{H}} = \underbrace{\sum_{\ell=1}^{L} \boldsymbol{g}_\ell \sqrt{p_\ell^{\mathrm{H}}} s_\ell^{\mathrm{H}}}_{\substack{\text{desired signal}\\ \text{\& intracell interference}}} + \underbrace{\boldsymbol{G}\sum_{k=1}^{K} \boldsymbol{w}_k s_k^{\mathrm{M}}}_{\text{DL-to-UL interference}} + \underbrace{\boldsymbol{n}_\ell^{\mathrm{H}}}_{\text{noise}} \quad (5)$$

where the transmit signal from the ℓth HTD is represented by $s_\ell^H \in \mathbb{C}$, the channel from the ℓth HTD to the UL BS is denoted by $\boldsymbol{g}_\ell \in \mathbb{C}^{N_r^U \times 1}$, the interfering channel from the DL BS to the UL BS is given by $\boldsymbol{G} \in \mathbb{C}^{N_r^U \times N_t^D}$, and $\boldsymbol{n}_\ell^H$ is the AWGN with distribution $\mathcal{CN}(0, (\sigma_\ell^{\mathrm{H}})^2 \boldsymbol{I})$. Then, the SINR for the ℓth UL HTD after applying the receive beamforming vector $\boldsymbol{v}_\ell \in \mathbb{C}^{N_r^U \times 1}$ is given by

$$\mathrm{SINR}_\ell^H = \frac{p_\ell^H |\boldsymbol{v}_\ell^{\dagger}\boldsymbol{g}_\ell|^2}{\sum_{j\neq\ell}^{L} p_j^H |\boldsymbol{v}_\ell^{\dagger}\boldsymbol{g}_j|^2 + \sum_{k=1}^{K} |\boldsymbol{v}_\ell^{\dagger}\boldsymbol{G}\boldsymbol{w}_k|^2 + (\widetilde{\sigma}_\ell^{\mathrm{H}})^2} \quad (6)$$

where $(\widetilde{\sigma}_\ell^{\mathrm{H}})^2 = (\sigma_\ell^{\mathrm{H}})^2 \|\boldsymbol{v}_\ell\|^2$.

III. Problem Formulation

We consider two related problems in the framework of green dynamic TDD networks. We first address a simplified problem where each device is assumed having no EH capabilities, and then a general problem where each device has EH capabilities as described in the general system model in Section II. The design objective for the simplified problem is per HTD/MTD QoS constrained power minimization, by optimizing the transceiver beamforming and the transmit power allocation from the UL HTD. The design problem, termed the JBPA optimization problem, is mathematically expressed as

$$\min_{\substack{\{\boldsymbol{w}_k\},\{\boldsymbol{v}_\ell\},\\ \{p_\ell^H \geq 0\}}} \sum_{k=1}^{K} \|\boldsymbol{w}_k\|^2 + \sum_{\ell=1}^{L} p_\ell^H \quad (7a)$$

$$\text{s.t.} \ \frac{|\boldsymbol{h}_k^{\dagger}\boldsymbol{w}_k|^2}{\sum_{i\neq k}^{K} |\boldsymbol{h}_k^{\dagger}\boldsymbol{w}_i|^2 + \sum_{\ell=1}^{L} |h_{k,\ell}|^2 p_\ell^H + (\sigma_k^{\mathrm{M}})^2} \geq \gamma_k^M \ \forall k \quad (7b)$$

$$\frac{p_\ell^H |\boldsymbol{v}_\ell^{\dagger}\boldsymbol{g}_\ell|^2}{\sum_{j\neq\ell}^{L} p_j^H |\boldsymbol{v}_\ell^{\dagger}\boldsymbol{g}_j|^2 + \sum_{k=1}^{K} |\boldsymbol{v}_\ell^{\dagger}\boldsymbol{G}\boldsymbol{w}_k|^2 + (\widetilde{\sigma}_\ell^{\mathrm{H}})^2} \geq \gamma_\ell^H \ \forall \ell \quad (7c)$$

where we have used $\rho_k = 1$ and $\widetilde{\sigma}_k^2 = 0 \ \forall k \in \mathcal{K}$ (i.e., each MTD has no EH capabilities and full received power is devoted to ID), and γ_k^M and γ_ℓ^H specify the preset target SINR for the kth MTD and ℓth HTD, respectively. Due to the dynamic TDD system [1], [29], [30], we consider the power of BS (DL) and machine (UL) in the objective function. Recently, 5G and 6G are small cell deployments. Therefore, this article's formulated problem and algorithm applies not only to the macrocell but also to the femtocell. In addition, minimizing the total transmit power in the objective function helps reduce CO_2 emissions (green communication) since too many devices and small cells simultaneously operate in a 5G/6G world [33].

The general problem has the same design objective and constraints, yet with an additional EH constraint and the receive PS ratio optimization at each MTD. The design problem, termed the joint beamforming, power allocation, and EH (JBPAEH) optimization problem, is mathematically expressed as

$$\min_{\substack{\{\boldsymbol{w}_k\},\{\boldsymbol{v}_\ell\},\\ \{\rho_k\},\{p_\ell^H\geq 0\}}} \sum_{k=1}^{K}\|\boldsymbol{w}_k\|^2+\sum_{\ell=1}^{L}p_\ell^H \tag{8a}$$

$$\text{s.t. } \frac{\rho_k|\boldsymbol{h}_k^\dagger\boldsymbol{w}_k|^2}{\rho_k\left(\sum_{i\neq k}^{K}|\boldsymbol{h}_k^\dagger\boldsymbol{w}_i|^2+\sum_{\ell=1}^{L}|h_{k,\ell}|^2p_\ell^H+(\sigma_k^{\mathrm{M}})^2\right)+\widetilde{\sigma}_k^2}\geq\gamma_k^M\ \forall k \tag{8b}$$

$$\frac{p_\ell^H|\boldsymbol{v}_\ell^\dagger\boldsymbol{g}_\ell|^2}{\sum_{j\neq\ell}^{L}p_j^H|\boldsymbol{v}_\ell^\dagger\boldsymbol{g}_j|^2+\sum_{k=1}^{K}|\boldsymbol{v}_\ell^\dagger\boldsymbol{G}\boldsymbol{w}_k|^2+(\widetilde{\sigma}_\ell^{\mathrm{H}})^2}\geq\gamma_\ell^H\ \forall\ell \tag{8c}$$

$$(1-\rho_k)\left(\sum_{i=1}^{K}|\boldsymbol{h}_k^\dagger\boldsymbol{w}_i|^2+\sum_{\ell=1}^{L}|h_{k,\ell}|^2p_\ell^H+(\sigma_k^{\mathrm{M}})^2\right)\geq E_k^M\ \forall k \tag{8d}$$

$$0\leq\rho_k\leq 1\ \forall k\in\mathcal{K} \tag{8e}$$

where (8d) specifies the minimum level of harvested energy at the kth MTD, E_k^M, assuming, without loss of generality, $\xi_k^M=1\ \forall k$, and (8e) specifies the legitimate range of the PS ratio for each MTD.

Both of the considered problems are challenging nonconvex coupled problems. Though the problems (7) and (8) are formulated for a single time instance in the TDD setting (i.e., one cell serves UL HTDs with the other serving DL MTDs), we notice that the problem formulation can be equivalently transformed to handle the other reversed direction in TDD (i.e., one cell serves DL HTDs with the other serving UL MTDs).[1] Moreover, the formulated problem and algorithm in this article also can deal with only MTD users in DL and UL (or HTD users in DL and UL) case, if a telephone company wants to deal with the pure IoT communication in 6G dynamic TDD issues [24].

In conventional TDD systems, the UL power allocation and DL transmit beamforming can be processed separately. In dynamic TDD systems, however, UL power allocation and the transceiver beamforming variables are coupled in the constraints in the JBPA problem (7), and the UL power allocation, transceiver beamforming, and PS ratios are coupled in the constraints in the JBPAEH problem (8), due to the new cross-link interference introduced by dynamic TDD [i.e., the third term in (1) and the second term in (5)]. We propose alternating optimization (AO)-based algorithms to tackle these challenging problems. Due to the different nature of the two problems, the solutions to the two problems are however different and one is not a straightforward extension of the other. More specifically, the structural properties of the additional EH constraint and PS ratio constraint in (8d) and (8e) render an efficient solution to problem (7) not applicable to problem (8). Thus, the proposed solutions to each problem present their own merits in the framework of each problem. The solution methods for problems (7) and (8) are presented in the next two sections, respectively.

[1]Problems (7) and (8) can be easily redefined to handle the reversed direction in TDD (i.e., one cell serves DL HTDs with the other serving UL MTDs). Specifically, for (7), the notations $(p_\ell^H,\sigma_k^M,\gamma_k^M,\widetilde{\sigma}_\ell^{\mathrm{H}},\gamma_\ell^H)$ can be changed as $(p_\ell^M,\sigma_k^H,\gamma_k^H,\widetilde{\sigma}_\ell^{\mathrm{M}},\gamma_\ell^M)$; note that we still have $K=L$. Similarly, for (8), the notations $(\widetilde{\sigma}_k,E_k^M)$ can be changed as $(\widetilde{\sigma}_k,E_k^H)$. For both changes above, one can observe that the optimization problem structures remain unaltered, meaning that the algorithms developed in the subsequent sections are still applicable for all the dynamic TDD time instances.

IV. Solving the JBPA Problem (7)

In this section, we present three approaches to solve problem (7).

A. SDR-Based AO Algorithm

Fixing all the UL beamforming $\{\boldsymbol{v}_\ell\}$, problem (7) can be reformulated as a semidefinite programming (SDP) problem, and when the DL beamforming $\{\boldsymbol{w}_k\}$ and UL HTD's power $\{p_\ell^H\}$ are fixed, $\{\boldsymbol{v}_\ell\}$ has a simple closed-form expression. Thus, the AO procedure is employed, which involves solving the following two subproblems iteratively.

1) Subproblem 1: Here, we fix $\{\boldsymbol{v}_\ell\}$ when solving problem (7). The resulting problem is still nonconvex and is convexified using the SDR technique [34]. Letting $\boldsymbol{W}_k=\boldsymbol{w}_k\boldsymbol{w}_k^\dagger$ and dropping the rank-one constraint $\mathrm{Rank}(\boldsymbol{W}_k)=1$, the SDR of problem (7) is given by

$$\min_{\substack{\{\boldsymbol{W}_k\succeq 0\},\\ \{p_\ell^H\geq 0\}}} \sum_{k=1}^{K}\mathrm{Tr}(\boldsymbol{W}_k)+\sum_{\ell=1}^{L}p_\ell^H \tag{9a}$$

$$\text{s.t. } \frac{\boldsymbol{h}_k^\dagger\boldsymbol{W}_k\boldsymbol{h}_k}{\gamma_k^M}-\sum_{i\neq k}^{K}\boldsymbol{h}_k^\dagger\boldsymbol{W}_i\boldsymbol{h}_k\geq\sum_{\ell=1}^{L}|h_{k,\ell}|^2p_\ell^H+(\sigma_k^{\mathrm{M}})^2\ \forall k \tag{9b}$$

$$\frac{p_\ell^H|\boldsymbol{v}_\ell^\dagger\boldsymbol{g}_\ell|^2}{\gamma_\ell^H}-\sum_{j\neq\ell}^{L}p_j^H|\boldsymbol{v}_\ell^\dagger\boldsymbol{g}_j|^2\geq\sum_{k=1}^{K}\xi_{\ell,k}+(\widetilde{\sigma}_\ell^{\mathrm{H}})^2\ \forall\ell \tag{9c}$$

where $\xi_{\ell,k}=\boldsymbol{v}_\ell^\dagger\boldsymbol{G}\boldsymbol{W}_k\boldsymbol{G}^\dagger\boldsymbol{v}_\ell$. Problem (9) is a standard SDR problem which can be solved by convex solvers, e.g., CVX [35].

The following theorem establishes that the optimal solution $\{\boldsymbol{W}_k\}$ to problem (9) is always rank one. Thus, the SDR approach preserves optimality.

Theorem 1: Let $\gamma_k^M>0$ and $\gamma_\ell^H>0$, the optimal beamforming solution $\boldsymbol{W}_k^*$ of problem (9) is always rank one, i.e., $\mathrm{Rank}(\boldsymbol{W}_k^*)=1\ \forall k$.

Proof: See Appendix A. ■

2) Subproblem 2: Here, we fix $\{\boldsymbol{w}_k\}$ and $\{p_\ell^H\}$ when solving problem (7). The optimal $\{\boldsymbol{v}_\ell\}$ that maximizes the UL SINR is the well-known MMSE receiver [36], [37], i.e.,

$$\boldsymbol{v}_\ell=\boldsymbol{R}^{-1}(\boldsymbol{w},\boldsymbol{p}^H)\boldsymbol{g}_\ell\sqrt{p_\ell^H} \tag{10}$$

where $\boldsymbol{R}(\boldsymbol{w},\boldsymbol{p}^H)=\sum_{j=1}^{L}p_j^H\boldsymbol{g}_j\boldsymbol{g}_j^\dagger+\sum_{k=1}^{K}\boldsymbol{G}\boldsymbol{w}_k\boldsymbol{w}_k^\dagger\boldsymbol{G}^\dagger+(\sigma_\ell^{\mathrm{H}})^2\boldsymbol{I}$, and $\boldsymbol{w}$ and $\boldsymbol{p}^H$ express the DL beamforming and UL HTD's power for all corresponding devices, respectively.

B. SOCP-Based AO Algorithm

The SOCP-based AO algorithm involves solving the following two subproblems iteratively.

1) Subproblem 1: Here, we fix $\{\boldsymbol{v}_\ell\}$ when solving problem (7). The resulting (nonconvex) problem can be equivalently transformed into the following convex SOCP problem, by a change of variables $\widetilde{p}_\ell^H = \sqrt{p_\ell^H}\ \forall \ell$

$$\min_{\substack{\{\widetilde{p}_\ell^H \geq 0\},\\ \{\boldsymbol{w}_k\}}} \sum_{k=1}^{K} \|\boldsymbol{w}_k\|^2 + \sum_{\ell=1}^{L} (\widetilde{p}_\ell^H)^2 \tag{11a}$$

$$\text{s.t. } \frac{\boldsymbol{h}_k^\dagger \boldsymbol{w}_k}{\sqrt{\gamma_k^M}} \geq \sqrt{\sum_{i\neq k}^{K} |\boldsymbol{h}_k^\dagger \boldsymbol{w}_i|^2 + \sum_{\ell=1}^{L} |h_{k,\ell}|^2 (\widetilde{p}_\ell^H)^2 + (\sigma_k^{\mathrm{M}})^2}\ \forall k \tag{11b}$$

$$\frac{\widetilde{p}_\ell^H \sqrt{\alpha_{\ell,\ell}}}{\sqrt{\gamma_\ell^H}} \geq \sqrt{\sum_{j\neq \ell}^{L} (\widetilde{p}_j^H)^2 \alpha_{\ell,j} + \sum_{k=1}^{K} |\boldsymbol{v}_\ell^\dagger \boldsymbol{G} \boldsymbol{w}_k|^2 + (\widetilde{\sigma}_\ell^{\mathrm{H}})^2}\ \forall \ell \tag{11c}$$

$$\mathrm{Re}(\boldsymbol{h}_k^\dagger \boldsymbol{w}_k) \geq 0\ \forall k \tag{11d}$$

$$\mathrm{Im}(\boldsymbol{h}_k^\dagger \boldsymbol{w}_k) = 0\ \forall k \tag{11e}$$

where $\alpha_{\ell,j} = |\boldsymbol{v}_\ell^\dagger \boldsymbol{g}_j|^2$. Note that, the amplitude of the beamforming vectors will not be affected by an arbitrary phase rotation. Thus, we let the complex vector $\boldsymbol{h}_k^\dagger \boldsymbol{w}_k$ be real in (11d) and (11e) [36], [38], [39].

2) Subproblem 2: Here, we fix $\{\boldsymbol{w}_k\}$ and $\{p_\ell^H\}$ when solving problem (7). The optimal $\{\boldsymbol{v}_\ell\}$ is the MMSE receiver (10).

C. UDD-Based AO Algorithm

The SDR-based and SOCP-based AO algorithms are based on solving a convex optimization problem using the interior point method, which could incur high computational complexity for massive-scale device communications. Here, we propose a UDD-based approach of low computational complexity [36], [37]. The UDD under the beamforming context was first shown by Rashid-Farrokhi *et al.* [40]. Later, Yu and Lan [41] showed the bridge between the UDD and convex optimization theory via Lagrangian. The method of UDD is to deal with the problem to transform from DL to UL. The difference between the conventional UDD-based design and this article is that we have considered UL and DL constraints simultaneously, as depicted in Fig. 2. In other words, the transmit beamforming will be transformed into the receive beamforming, and *vice versa*. Fortunately, the UDD method via Lagrangian dual is also useful to handle the hard JBPA problem in this article. The proposed method is elaborated in the following.

Based on the AO procedure, we first fix $\{\boldsymbol{v}_\ell\}$ when solving problem (7). By expressing $\boldsymbol{w}_k$ as $\boldsymbol{w}_k = \sqrt{p_k^M}\widetilde{\boldsymbol{w}}_k$, where p_k^M and $\widetilde{\boldsymbol{w}}_k$ denote the power and direction of $\boldsymbol{w}_k$, respectively, and $\|\widetilde{\boldsymbol{w}}_k\| = 1$ without loss of generality, we can rewrite the resulting problem as

$$\min_{\substack{\{p_k^M \geq 0\}\\ \{p_\ell^H \geq 0\}}} \sum_{k=1}^{K} p_k^M + \sum_{\ell=1}^{L} p_\ell^H \tag{12a}$$

$$\text{s.t. } \frac{p_k^M |\boldsymbol{h}_k^\dagger \widetilde{\boldsymbol{w}}_k|^2}{\sum_{i\neq k}^{K} p_i^M |\boldsymbol{h}_k^\dagger \widetilde{\boldsymbol{w}}_i|^2 + \sum_{\ell=1}^{L} |h_{k,\ell}|^2 p_\ell^H + (\sigma_k^{\mathrm{M}})^2} \geq \gamma_k^M\ \forall k \tag{12b}$$

$$\frac{p_\ell^H |\boldsymbol{v}_\ell^\dagger \boldsymbol{g}_\ell|^2}{\sum_{j\neq \ell}^{L} p_j^H |\boldsymbol{v}_\ell^\dagger \boldsymbol{g}_j|^2 + \sum_{k=1}^{K} p_k^M |\boldsymbol{v}_\ell^\dagger \boldsymbol{G} \widetilde{\boldsymbol{w}}_k|^2 + (\widetilde{\sigma}_\ell^{\mathrm{H}})^2} \geq \gamma_\ell^H\ \forall \ell. \tag{12c}$$

Then, the UDD technique is used to solve problem (12). Specifically, problem (12) is solved via its dual problem, which is given by

$$\max_{\substack{\{\lambda_k^M \geq 0\}\\ \{\lambda_\ell^H \geq 0\}}} \sum_{k=1}^{K} \lambda_k^M (\sigma_k^{\mathrm{M}})^2 + \sum_{\ell=1}^{L} \lambda_\ell^H (\widetilde{\sigma}_\ell^{\mathrm{H}})^2 \tag{13a}$$

$$\text{s.t. } \frac{\lambda_k^M |\boldsymbol{h}_k^\dagger \widetilde{\boldsymbol{w}}_k|^2}{\sum_{i\neq k}^{K} \lambda_i^M |\boldsymbol{h}_i^\dagger \widetilde{\boldsymbol{w}}_k|^2 + \sum_{\ell=1}^{L} \lambda_\ell^H |\boldsymbol{v}_\ell^\dagger \boldsymbol{G} \widetilde{\boldsymbol{w}}_k|^2 + 1} \leq \gamma_k^M\ \forall k \tag{13b}$$

$$\frac{\lambda_\ell^H |\boldsymbol{v}_\ell^\dagger \boldsymbol{g}_\ell|^2}{\sum_{j\neq \ell}^{L} \lambda_j^H |\boldsymbol{v}_j^\dagger \boldsymbol{g}_\ell|^2 + \sum_{k=1}^{K} |h_{k,\ell}|^2 \lambda_k^M + 1} \leq \gamma_\ell^H\ \forall \ell \tag{13c}$$

where λ_k^M and λ_ℓ^H are the Lagrange multipliers of problem (12).

Since problem (12) is a linear programming (LP) problem, Slater's condition is satisfied and the duality gap is zero [36]. To see that problem (13) is the dual problem of problem (12), first we have the Lagrangian of problem (12)

$$\begin{aligned}\mathcal{L}(\boldsymbol{p}^M, \boldsymbol{p}^H, \boldsymbol{\lambda}^M, \boldsymbol{\lambda}^H) &= \sum_{k=1}^{K} p_k^M + \sum_{\ell=1}^{L} p_\ell^H + \sum_{k=1}^{K} \lambda_k^M \\ &\times \left(\sum_{i\neq k}^{K} p_i^M |\boldsymbol{h}_k^\dagger \widetilde{\boldsymbol{w}}_i|^2 + \sum_{\ell=1}^{L} |h_{k,\ell}|^2 p_\ell^H + (\sigma_k^{\mathrm{M}})^2 - \frac{p_k^M}{\gamma_k^M} |\boldsymbol{h}_k^\dagger \widetilde{\boldsymbol{w}}_k|^2 \right) \\ &+ \sum_{\ell=1}^{L} \lambda_\ell^H \left(\sum_{j\neq \ell}^{L} p_j^H |\boldsymbol{v}_\ell^\dagger \boldsymbol{g}_j|^2 + \sum_{k=1}^{K} p_k^M |\boldsymbol{v}_\ell^\dagger \boldsymbol{G} \widetilde{\boldsymbol{w}}_k|^2 + (\widetilde{\sigma}_\ell^{\mathrm{H}})^2 \right. \\ &\left. - \frac{p_\ell^H}{\gamma_\ell^H} |\boldsymbol{v}_\ell^\dagger \boldsymbol{g}_\ell|^2 \right)\end{aligned} \tag{14}$$

where $\boldsymbol{p}^M, \boldsymbol{p}^H, \boldsymbol{\lambda}^M$, and $\boldsymbol{\lambda}^H$ denote $p_k^M, p_\ell^H, \lambda_k^M$, and λ_ℓ^H for all corresponding devices, respectively. Then, rearranging the terms of (14) yields

$$\begin{aligned}\mathcal{L}(\boldsymbol{p}^M, \boldsymbol{p}^H, \boldsymbol{\lambda}^M, \boldsymbol{\lambda}^H) &= \sum_{k=1}^{K} \lambda_k^M (\sigma_k^{\mathrm{M}})^2 + \sum_{\ell=1}^{L} \lambda_\ell^H (\widetilde{\sigma}_\ell^{\mathrm{H}})^2 \\ &+ \sum_{k=1}^{K} p_k^M \left(1 + \sum_{i\neq k}^{K} \lambda_i^M |\boldsymbol{h}_i^\dagger \widetilde{\boldsymbol{w}}_k|^2 + \sum_{\ell=1}^{L} \lambda_\ell^H \zeta_{\ell,k} - \frac{\lambda_k^M}{\gamma_k^M} |\boldsymbol{h}_k^\dagger \widetilde{\boldsymbol{w}}_k|^2 \right) \\ &+ \sum_{\ell=1}^{L} p_\ell^H \left(1 + \sum_{j\neq \ell}^{L} \lambda_j^H |\boldsymbol{v}_j^\dagger \boldsymbol{g}_\ell|^2 + \sum_{k=1}^{K} |h_{k,\ell}|^2 \lambda_k^M - \frac{\lambda_\ell^H}{\gamma_\ell^H} |\boldsymbol{v}_\ell^\dagger \boldsymbol{g}_\ell|^2 \right)\end{aligned} \tag{15}$$

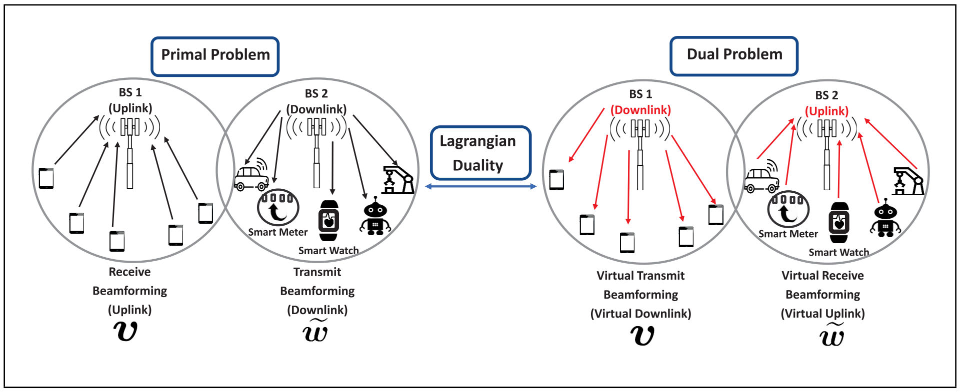

Fig. 2. Dual of dynamic TDD system via Lagrangian dual method. By the Lagrangian method, the transmit beamforming $\{\widetilde{\boldsymbol{w}}\}$ can be transformed to virtual receive beamforming $\{\boldsymbol{v}\}$, and *vice versa*.

where $\zeta_{\ell,k} = |\boldsymbol{v}_\ell^\dagger \boldsymbol{G}\widetilde{\boldsymbol{w}}_k|^2$. In order to avoid the unbound variables in (15), the third and fourth terms of (15) in parentheses must be nonnegative (otherwise, there exists a set of $\{\boldsymbol{p}^M, \boldsymbol{p}^H\}$ that will make the dual objective $g(\boldsymbol{\lambda}^M, \boldsymbol{\lambda}^H) = \min_{\boldsymbol{p}^M, \boldsymbol{p}^H} \mathcal{L}(\boldsymbol{p}^M, \boldsymbol{p}^H, \boldsymbol{\lambda}^M, \boldsymbol{\lambda}^H)$ become minus infinity), it is established that the dual problem of (12) is given by (13).

Due to the duality property, we can obtain the optimal beamforming direction of (12) from (13), as shown in the following theorem.

Theorem 2: In the dual problem (13), the virtual receive beamforming can be obtained by following MMSE problem [36]–[38]

$$\min_{\{s_i^M\}} \quad \mathbb{E}\{|\widetilde{\boldsymbol{w}}_k^\dagger \boldsymbol{y} - s_i^M|^2\}$$

where $\boldsymbol{y} = \sum_{i=1}^K \boldsymbol{h}_i \sqrt{\lambda_i^M} s_i^M + \boldsymbol{G}^\dagger \sum_{\ell=1}^L \boldsymbol{v}_\ell \sqrt{\lambda_\ell^H} s_\ell^H + 1$. The solution of the MMSE problem can be obtained by

$$\widetilde{\boldsymbol{w}}_k^\star = \frac{\boldsymbol{Q}^{-1}(\boldsymbol{\lambda}^M, \boldsymbol{\lambda}^H)\boldsymbol{h}_k\sqrt{\lambda_k^M}}{\|\boldsymbol{Q}^{-1}(\boldsymbol{\lambda}^M, \boldsymbol{\lambda}^H)\boldsymbol{h}_k\sqrt{\lambda_k^M}\|} \; \forall k \tag{16}$$

where $\boldsymbol{Q}(\boldsymbol{\lambda}^M, \boldsymbol{\lambda}^H) = \sum_{i=1}^K \lambda_i^M \boldsymbol{h}_i \boldsymbol{h}_i^\dagger + \sum_{\ell=1}^L \lambda_\ell^H \boldsymbol{G}^\dagger \boldsymbol{v}_\ell \boldsymbol{v}_\ell^\dagger \boldsymbol{G} + \boldsymbol{I}$ [36]. Moreover, the optimal beamforming direction of (12) is the dual MMSE solution.

Proof: If problems (12) and (13) are in the convex form, the KKT necessary conditions are also sufficient for optimality. It is observed that the structure and KKT conditions are the same for (12) and (13). Thus, (16) holds. ■

Note that, the relationship between the primal beamforming direction of (7) and the dual beamforming direction of (12) is as follows [36]–[38], [42]:

$$\frac{\boldsymbol{w}_k^\star}{\|\boldsymbol{w}_k^\star\|} = \frac{\widetilde{\boldsymbol{w}}_k^\star}{\|\widetilde{\boldsymbol{w}}_k^\star\|}.$$

It is worth noting that we only use the dual MMSE (16) in Algorithm 1. Subproblem 2 is used for Algorithm 2 (also for SDR (9), SOCP (11) in JBPA and SDR (25) in JBPAEH).

Using the classical fixed-point method [37], [43], the dual problem (13) can be funded by the fixed-point iteration method. Interestingly, (13b) and (13c) can be achieved the equality at the optimum. Therefore, (13b) and (13c) can be rewritten as

$$\begin{aligned} \lambda_k^M &= \mathcal{F}_k^M(\boldsymbol{\lambda}^M, \boldsymbol{\lambda}^H) \\ &\triangleq \frac{1}{\boldsymbol{h}_k^\dagger \boldsymbol{Q}^{-1}(\boldsymbol{\lambda}^M, \boldsymbol{\lambda}^H)\boldsymbol{h}_k(1 + \frac{1}{\gamma_k^M})} \; \forall k \qquad (17a) \\ \lambda_\ell^H &= \mathcal{F}_\ell^H(\boldsymbol{\lambda}^M, \boldsymbol{\lambda}^H) \\ &\triangleq \frac{\sum_{j=1}^L \lambda_j^H |\boldsymbol{v}_j^\dagger \boldsymbol{g}_\ell|^2 + \sum_{k=1}^K |h_{k,\ell}|^2 \lambda_k^M + 1}{|\boldsymbol{v}_\ell^\dagger \boldsymbol{g}_\ell|^2(1 + \frac{1}{\gamma_\ell^H})} \; \forall \ell. \qquad (17b) \end{aligned}$$

The convergence and optimality of fixed-point iteration are summarized in the following theorem.

Theorem 3: Define $\boldsymbol{\mathcal{F}}(\boldsymbol{\lambda}^M, \boldsymbol{\lambda}^H) \triangleq [\mathcal{F}_1^M(\boldsymbol{\lambda}^M, \boldsymbol{\lambda}^H), \ldots, \mathcal{F}_K^M(\boldsymbol{\lambda}^M, \boldsymbol{\lambda}^H), \mathcal{F}_1^H(\boldsymbol{\lambda}^M, \boldsymbol{\lambda}^H), \ldots, \mathcal{F}_L^H(\boldsymbol{\lambda}^M, \boldsymbol{\lambda}^H)]^\top$ and fixed-point equation can be written as

$$\boldsymbol{\lambda} = \begin{bmatrix} \boldsymbol{\lambda}^M \\ \boldsymbol{\lambda}^H \end{bmatrix} = \boldsymbol{\mathcal{F}}(\boldsymbol{\lambda}^M, \boldsymbol{\lambda}^H). \tag{18}$$

Suppose problem (13) is feasible. The standard fixed-point function of (18) satisfies the property of positivity, monotonicity, and scalability as [37], [43].

1) *Positivity:* If $\boldsymbol{\lambda}^M > 0$ and $\boldsymbol{\lambda}^H > 0$, then $\mathcal{F}_k^M(\boldsymbol{\lambda}^M, \boldsymbol{\lambda}^H) > 0 \; \forall k$, and $\mathcal{F}_\ell^H(\boldsymbol{\lambda}^M, \boldsymbol{\lambda}^H) > 0 \; \forall \ell$.
2) *Monotonicity:* If $\boldsymbol{\lambda}^M > (\boldsymbol{\lambda}^M)'$ and $\boldsymbol{\lambda}^H > (\boldsymbol{\lambda}^H)'$, then $\mathcal{F}_k^M(\boldsymbol{\lambda}^M, \boldsymbol{\lambda}^H) > \mathcal{F}_k^M((\boldsymbol{\lambda}^M)', (\boldsymbol{\lambda}^H)') \; \forall k$, and $\mathcal{F}_\ell^H(\boldsymbol{\lambda}^M, \boldsymbol{\lambda}^H) > \mathcal{F}_\ell^H((\boldsymbol{\lambda}^M)', (\boldsymbol{\lambda}^H)') \; \forall \ell$.
3) *Scalability:* For all $\alpha > 1$, $\alpha\mathcal{F}_k^M(\boldsymbol{\lambda}^M, \boldsymbol{\lambda}^H) > \mathcal{F}_k^M(\alpha\boldsymbol{\lambda}^M, \alpha\boldsymbol{\lambda}^H) \; \forall k$, and $\alpha\mathcal{F}_\ell^H(\boldsymbol{\lambda}^M, \boldsymbol{\lambda}^H) > \mathcal{F}_\ell^H(\alpha\boldsymbol{\lambda}^M, \alpha\boldsymbol{\lambda}^H) \; \forall \ell$.

Then, (18) converges to the unique fixed point. Due to the uniqueness and convexity of (13), the optimality of (13) is seen.

Proof: See Appendix B. ■

We propose the UDD-Based AO Algorithm to deal with problem (12) in Algorithm 1. First, $\{\boldsymbol{v}_\ell\}$ of problem (13) is fixed. Then, the fixed-point in (18) can be solved by iterative method. When the dual power $\{\boldsymbol{\lambda}^H\}$ and $\{\boldsymbol{\lambda}^M\}$ are obtained by the iterative fixed-point method, we can solve the dual MMSE direction solution in (16). Finally, the power of primal problem (12) can also obtained by iterative fixed-point

Algorithm 1 UDD-Based AO Algorithm for Problem (7): Low-Complexity Optimal Design

Initialization: Given UL beamforming $\{\boldsymbol{v}_\ell^{(0)}\}\ \forall \ell$. $(\boldsymbol{\lambda}^{\mathrm{M}})^{(0)}$, $(\boldsymbol{\lambda}^{\mathrm{H}})^{(0)}$, $(\boldsymbol{p}^{\mathrm{M}})^{(0)}$, and $(\boldsymbol{p}^{\mathrm{H}})^{(0)}$; set $\tau \leftarrow 0$ and $t \leftarrow 0$.
repeat
  The dual fixed-point iteration (18) $[((\boldsymbol{\lambda}^{\mathrm{M}})^{(\tau+1)})^T\ ((\boldsymbol{\lambda}^{\mathrm{H}})^{(\tau+1)})^T]^T \leftarrow \boldsymbol{\mathcal{F}}((\boldsymbol{\lambda}^{\mathrm{M}})^{(\tau)}, (\boldsymbol{\lambda}^{\mathrm{H}})^{(\tau)})$.
  $\tau \leftarrow \tau + 1$
until (20) is satisfied.
Using $[(\boldsymbol{\lambda}^{\mathrm{M}})^{(\tau+1)}; (\boldsymbol{\lambda}^{\mathrm{H}})^{(\tau+1)}]$, obtained $\{\widetilde{\boldsymbol{w}}_k^\star\}$ by (16);
repeat
  The primal fixed-point iteration (19) $[((\boldsymbol{p}^{\mathrm{M}})^{(t+1)})^T\ ((\boldsymbol{p}^{\mathrm{H}})^{(t+1)})^T]^T \leftarrow \boldsymbol{\mathcal{F}}((\boldsymbol{p}^{\mathrm{M}})^{(t)}, (\boldsymbol{p}^{\mathrm{H}})^{(t)})$.
  $t \leftarrow t + 1$.
until (21) is satisfied.
$\boldsymbol{w}_k^\star \leftarrow \sqrt{(p_k^{\mathrm{M}})^\star}\,\widetilde{\boldsymbol{w}}_k^\star,\ \forall k \in \mathcal{K}$.

method. Similar to the method in the dual fixed-point method, the fixed-point solution to the problem (12) can be written as

$$p_k^M = \frac{\sum_{i=1}^K p_i^M |\boldsymbol{h}_k^\dagger \widetilde{\boldsymbol{w}}_i|^2 + \sum_{\ell=1}^L |h_{k,\ell}|^2 p_\ell^H + (\sigma_k^{\mathrm{M}})^2}{|\boldsymbol{h}_k^\dagger \widetilde{\boldsymbol{w}}_k|^2 (1 + \frac{1}{\gamma_k^M})}\ \forall k \quad (19a)$$

$$p_\ell^H = \frac{1}{\boldsymbol{g}_\ell^\dagger \widetilde{\boldsymbol{R}}^{-1}(\boldsymbol{p}^M, \boldsymbol{p}^H, \widetilde{\boldsymbol{w}}) \boldsymbol{g}_\ell (1 + \frac{1}{\gamma_\ell^H})}\ \forall \ell \quad (19b)$$

where $\widetilde{\boldsymbol{R}}(\boldsymbol{p}^M, \boldsymbol{p}^H, \widetilde{\boldsymbol{w}}) = \sum_{j=1}^L p_j^H \boldsymbol{g}_j \boldsymbol{g}_j^\dagger + \sum_{k=1}^K p_k^M \boldsymbol{G} \widetilde{\boldsymbol{w}}_k \widetilde{\boldsymbol{w}}_k^\dagger \boldsymbol{G}^\dagger + (\sigma_\ell^{\mathrm{H}})^2 \boldsymbol{I}$. In Algorithm 1, the stopping criterion of the fixed-point method (18) is given by

$$\text{The stopping criterion} = \frac{\|\boldsymbol{\lambda}_{\mathrm{opt}}^{\star\,(\tau+1)} - \boldsymbol{\lambda}_{\mathrm{opt}}^{\star\,(\tau)}\|}{\|\boldsymbol{\lambda}_{\mathrm{opt}}^{\star\,(\tau)}\|} < \epsilon_1 \quad (20)$$

where $\boldsymbol{\lambda}_{\mathrm{opt}}^{\star\,(\tau+1)}$ and $\boldsymbol{\lambda}_{\mathrm{opt}}^{\star\,(\tau)}$ represent the optimal results of (18) at the $(\tau+1)$th and τth iterations, respectively, and the stopping criterion is ϵ_1. Similarly, let $\boldsymbol{p} = [(\boldsymbol{p}^M)^T\ (\boldsymbol{p}^H)^T]^\top$. The stopping criterion of (19) is given by

$$\text{The stopping criterion} = \frac{\|\boldsymbol{p}_{\mathrm{opt}}^{\star\,(t+1)} - \boldsymbol{p}_{\mathrm{opt}}^{\star\,(t)}\|}{\|\boldsymbol{p}_{\mathrm{opt}}^{\star\,(t)}\|} < \epsilon_2 \quad (21)$$

where the optimal results at the $(t+1)$th and tth iterations are $\boldsymbol{p}_{\mathrm{opt}}^{\star\,(t+1)}$ and $\boldsymbol{p}_{\mathrm{opt}}^{\star\,(t)}$, respectively, and the stopping criterion is ϵ_2. Algorithm 1 summarizes the proposed algorithm.

D. Computational Complexity

In constrained optimization problems, the computational complexity consists of two parts: 1) the iteration complexity and 2) the per-iteration computational cost [1], [44]. The complexities are computed as follows. For the SDR-based AO method (JBPA), the computational complexity of solving the SDR problem (9) using an interior-point-method (IPM) and calculating the MMSE solution (10) using the matrix inversion is given by

$$\underbrace{\sqrt{(2K+L)}}_{\text{Iteration Complexity}} \cdot \mathcal{O}\left(I\left(\underbrace{K(N_t^D)^3}_{\text{Formation}} + \underbrace{(N_t^D)^3}_{\text{Factorization}} + \underbrace{L(N_r^U)^3}_{\text{MMSE}}\right)\right) = \sqrt{(2K+L)}\,\mathcal{O}\Big(I\Big((K+1)(N_t^D)^3 + L(N_r^U)^3\Big)\Big) \quad (22)$$

where I denotes the iteration number. For the SOCP-based AO method (JBPA), the computational complexity of solving the SOCP problem (11) can be written as

$$\underbrace{\sqrt{(K+L)}}_{\text{Iteration Complexity}} \cdot \mathcal{O}\left(I\left(\underbrace{K(N_t^D)^3 + L(N_r^U)^2}_{\text{Formation}} + \underbrace{(N_t^D)^2}_{\text{Factorization}} + \underbrace{L(N_r^U)^3}_{\text{MMSE}}\right)\right). \quad (23)$$

In the UDD-based AO method (JBPA), the computational complexity of the fixed point iteration method of (18) is given by $\mathcal{O}(K(N_t^D)^3)$ [42]. In (16), the dual MMSE is given by $\mathcal{O}(K(N_t^D)^3)$ [36], [37]. The computational complexity calculation in the fixed-point solution of the primal problem in (19) is given by $\mathcal{O}(L(N_r^U)^3)$. We summarize the computational complexities of the UDD method as

$$\mathcal{O}\left(I\left(\underbrace{K(N_t^D)^3}_{(18)} + \underbrace{K(N_t^D)^3}_{\text{MMSE}} + \underbrace{L(N_r^U)^3}_{(19)}\right)\right) = \mathcal{O}\Big(I\Big(2K(N_t^D)^3 + L(N_r^U)^3\Big)\Big). \quad (24)$$

From this analysis, one can see that only the number of antennas and the number of users will affect the computational complexity of the proposed UDD algorithm.

Since (23) and (24) are not clear in the Big-O (upper bound). Here, we analyze the Big-Omega (lower bound) of formation of the optimization theory. In Problem (9), the computational complexity of (9b) and (9c) are $K[(N_t^D)^3 + (N_t^D)^3 + L + 1]$ and $L[3 + L + (N_t^D)^3 + 1]$, respectively. Thus, the total computational complexity of SDR in the JBPA problem is given in Table I.[2] Also, in the Problem (11), the computational complexity of (11b) and (11c) are $K[(N_t^D)^3 + 1]$ and $L[(N_r^U)^2 + 1]$, respectively. Thus, the total computational complexity of SOCP in the JBPA problem is given in the Table I. Finally, the fixed point iteration of (17a) is dominated by the matrix inversion operation $K(N_t^D)^3$. The computational complexity of (17b) is $L + K + 1 + 1$. The total computational complexity of the fixed point iteration (17) [3] can be expressed as $K(N_t^D)^3 + L + K + 2$. Thus, the total computational complexity of Algorithm 1 is given in the Table I.

In general, the fixed point method is time efficient than SOCP (CVX) method even though the computational complexity theory is not apparent, similar to [42, Remark 2]. This is

[2]Note that we only analyze the formation of optimization theory since the factorization is fixed [44], and the MMSE in (22)–(24) are all dominated by the matrix inverse.

[3]Note that the function form of (17) is (18) in the manuscript.

because the CVX has more inner computational loops (IPM) than the pure closed-form method. It is observed that the computation complexity of SOCP (vector) is lower than SDR (matrix). The closed-form solution is much more time-efficient than CVX tool.

V. Solving the JBPAEH Problem (8)

In this section, we present two convex approaches to solve the JBPAEH problem (8), e.g., SDR and SOCP relaxation. The UDD-based AO algorithm can not use for the JBPAEH problem (8) due to the constraint (8d) and the PS variables $\rho_k\ \forall k$. Thus, we use the SDR and SOCP relaxation methods to deal with the JBPAEH problem (8).

A. SDR-Based AO Algorithm

1) Subproblem 1: Here, we fix $\{\boldsymbol{v}_\ell\}$ when solving problem (8). However, the resulting problem is still not convex and needs further processing using the SDR technique [34]. In SDR, the constraint Rank($\boldsymbol{W}_k$)= 1, where $\boldsymbol{W}_k = \boldsymbol{w}_k\boldsymbol{w}_k^\dagger$, is dropped in order to obtain the convexity of the problem. By dropping the rank-one constraint, problem (8) can be transformed to

$$\min_{\substack{\{\boldsymbol{W}_k\},\{p_\ell^H\},\\ \{0\le\rho_k\le 1\}}} \sum_{k=1}^{K}\mathrm{Tr}(\boldsymbol{W}_k)+\sum_{\ell=1}^{L}p_\ell^H \tag{25a}$$

$$\text{s.t. } \frac{\boldsymbol{h}_k^\dagger\boldsymbol{W}_k\boldsymbol{h}_k}{\gamma_k^M}-\sum_{i\neq k}^{K}\boldsymbol{h}_k^\dagger\boldsymbol{W}_i\boldsymbol{h}_k-\sum_{\ell=1}^{L}|h_{k,\ell}|^2p_\ell^H-(\sigma_k^{\mathrm{M}})^2\ge\frac{\widetilde{\sigma}_k^2}{\rho_k}\ \forall k \tag{25b}$$

$$\frac{p_\ell^H|\boldsymbol{v}_\ell^\dagger\boldsymbol{g}_\ell|^2}{\gamma_\ell^H}\ge\sum_{j\neq\ell}^{L}p_j^H|\boldsymbol{v}_\ell^\dagger\boldsymbol{g}_j|^2+\sum_{k=1}^{K}\boldsymbol{v}_\ell^\dagger\boldsymbol{G}\boldsymbol{W}_k\boldsymbol{G}^\dagger\boldsymbol{v}_\ell+(\widetilde{\sigma}_\ell^{\mathrm{H}})^2\ \forall\ell \tag{25c}$$

$$\sum_{i=1}^{K}\boldsymbol{h}_k^\dagger\boldsymbol{W}_i\boldsymbol{h}_k+\sum_{\ell=1}^{L}|h_{k,\ell}|^2p_\ell^H+(\sigma_k^{\mathrm{M}})^2\ge\frac{E_k^M}{(1-\rho_k)}\ \forall k. \tag{25d}$$

If the optimal solution $\{\boldsymbol{W}_k\}$ to problem (25) is rank one, then the optimal $\{\boldsymbol{w}_k\}$ can obtain from eigenvalue decomposition. Since the problem (25) always has the rank-one solution, we have the following theorem.

Theorem 4: Let $\gamma_k^M>0$, $\gamma_\ell^H>0$, and $E_k^M>0$, the optimal beamforming solution $\boldsymbol{W}_k^*$ of problem (25) is always rank one, i.e., Rank($\boldsymbol{W}_k^*$) $=1\ \forall k$.

Proof: See Appendix C. ■

The rank-one optimality of the SDR problem (25) is obtained by examining the KKT conditions of the problem. Due to the rank-one optimal solution, the SDR problem (25) has no loss of optimality.

2) Subproblem 2: Here, we fix $\{\boldsymbol{w}_k\}$ and $\{p_\ell^H\}$ when solving problem (8). The optimal $\{\boldsymbol{v}_\ell\}$ maximizing the UL SINR is the MMSE receiver (10).

Although the SDR method has a good rank-one structure, the matrix form comes at the cost of relatively high computational complexity. A low-complexity algorithm to solve problem (8) is presented as follows.

B. SOCP Relaxation-Based AO Algorithm

Due to constraints (8d) and (8e), problem (8) cannot be directly converted to an SOCP convex problem. Therefore, we utilize the relaxation method from [45]. First, problem (8) can be equivalently rewritten as

$$\min_{\substack{\{\boldsymbol{w}_k\},\{\boldsymbol{v}_\ell\},\\ \{\rho_k\},\{p_\ell^H\ge 0\}}} \sum_{k=1}^{K}\|\boldsymbol{w}_k\|^2+\sum_{\ell=1}^{L}p_\ell^H \tag{26a}$$

$$\text{s.t. } \frac{|\boldsymbol{h}_k^\dagger\boldsymbol{w}_k|^2}{\sum_{i\neq k}^{K}|\boldsymbol{h}_k^\dagger\boldsymbol{w}_i|^2+\sum_{\ell=1}^{L}|h_{k,\ell}|^2p_\ell^H+(\sigma_k^{\mathrm{M}})^2+\frac{\widetilde{\sigma}_k^2}{\alpha_k^2}}\ge\gamma_k^M\ \forall k \tag{26b}$$

$$\frac{p_\ell^H|\boldsymbol{v}_\ell^\dagger\boldsymbol{g}_\ell|^2}{\sum_{j\neq\ell}^{L}p_j^H|\boldsymbol{v}_\ell^\dagger\boldsymbol{g}_j|^2+\sum_{k=1}^{K}|\boldsymbol{v}_\ell^\dagger\boldsymbol{G}\boldsymbol{w}_k|^2+(\widetilde{\sigma}_\ell^{\mathrm{H}})^2}\ge\gamma_\ell^H\ \forall\ell \tag{26c}$$

$$\sum_{i=1}^{K}|\boldsymbol{h}_k^\dagger\boldsymbol{w}_i|^2+\sum_{\ell=1}^{L}|h_{k,\ell}|^2p_\ell^H+(\sigma_k^{\mathrm{M}})^2\ge\frac{E_k^M}{\beta_k^2}\ \forall k \tag{26d}$$

$$\alpha_k^2+\beta_k^2\le 1\ \forall k \tag{26e}$$

$$0\le\rho_k\le 1\ \forall k \tag{26f}$$

where all the constraints except (26e) follow directly from the constraints of problem (8) after rearranging terms. In (26e), let $\alpha_k^2=\rho_k$ and $\beta_k^2=1-\rho_k$, where $\alpha_k>0$ and $\beta_k>0$, and must satisfy the given condition with equality at the optimality [45], [46]. Next, we use the SOCP relaxation techniques to transform constraints (26b)–(26d), so that the hard problem can be transformed as a tractable convex (SOCP) optimization problem.

1) Constraint (26b): By change of variables $\widetilde{p}_\ell^H=\sqrt{p_\ell^H}\ \forall\ell$, constraints (26b) can be expressed as

$$\frac{|\boldsymbol{h}_k^\dagger\boldsymbol{w}_k|^2}{\gamma_k^M}-\sum_{i\neq k}^{K}|\boldsymbol{h}_k^\dagger\boldsymbol{w}_i|^2-\sum_{\ell=1}^{L}|h_{k,\ell}|^2(\widetilde{p}_\ell^H)^2\ge(\sigma_k^{\mathrm{M}})^2+\frac{\widetilde{\sigma}_k^2}{\alpha_k^2}. \tag{27}$$

In addition, we use another auxiliary variable $r_k>0\ \forall k$, such that $r_k^2=(\widetilde{\sigma}_k^2/\alpha_k^2)$, which implies $r_k=(\widetilde{\sigma}_k/\alpha_k)$ or $r_k\alpha_k=\widetilde{\sigma}_k$. Thus, constraint (26b) can be transformed as the following SOCP constraints:

$$\sqrt{\sum_{i\neq k}^{K}|\boldsymbol{h}_k^\dagger\boldsymbol{w}_i|^2+\sum_{\ell=1}^{L}|h_{k,\ell}|^2(\widetilde{p}_\ell^H)^2+(\sigma_k^{\mathrm{M}})^2+r_k^2}\le\frac{\boldsymbol{h}_k^\dagger\boldsymbol{w}_k}{\sqrt{\gamma_k^M}}\ \forall k \tag{28a}$$

$$\sqrt{(r_k-\alpha_k)^2+4\widetilde{\sigma}_k}\le r_k+\alpha_k\ \forall k \tag{28b}$$

$$\mathrm{Re}(\boldsymbol{h}_k^\dagger\boldsymbol{w}_k)\ge 0\ \forall k \tag{28c}$$

$$\mathrm{Im}(\boldsymbol{h}_k^\dagger\boldsymbol{w}_k)=0\ \forall k. \tag{28d}$$

From (27) to (28a), we take square roots on both sides of the inequality. Equation (28b) is a relaxation that follows from the property [45], [47] that if $ab\ge z^2$ (where $a,b\ge 0$) then

$$\sqrt{(a-b)^2+4z^2}\le a+b. \tag{29}$$

Now, (28) is a standard form for SOCP.

TABLE I
COMPLEXITY ANALYSIS OF THE CONVEX RESTRICTION FORMULATIONS AND PROPOSED METHOD

Method	Complexity Order of Big-Omega (JBPA Problem)
SDR (Problem (9))	$\underbrace{\sqrt{(2K+L)}}_{\text{Iteration Complexity}}\ \mathcal{O}\Big(I\Big(\underbrace{K[2(N_t^{\mathrm{D}})^3+L+1]+L[4+L+(N_t^{\mathrm{D}})^3]}_{\text{Formation}}+\underbrace{(N_t^{\mathrm{D}})^3}_{\text{Factorization}}+\underbrace{L(N_r^{\mathrm{U}})^3}_{\text{MMSE}}\Big)\Big)$
SOCP (Problem (11))	$\underbrace{\sqrt{(K+L)}}_{\text{Iteration Complexity}}\ \mathcal{O}\Big(I\Big(\underbrace{K[(N_t^{\mathrm{D}})^3+1]+L[(N_r^{\mathrm{U}})^2+1]}_{\text{Formation}}+\underbrace{(N_t^{\mathrm{D}})^2}_{\text{Factorization}}+\underbrace{L(N_r^{\mathrm{U}})^3}_{\text{MMSE}}\Big)\Big)$
Algorithm 1	$\mathcal{O}\Big(I\Big(\underbrace{K(N_t^{\mathrm{D}})^3+L+K+2}_{(18)}+\underbrace{K(N_t^{\mathrm{D}})^3}_{\text{MMSE}}+\underbrace{K+L+2+L(N_r^{\mathrm{U}})^3}_{(19)}\Big)\Big)$

2) Constraint (26c): Due to no any EH constraints (variables), (26c) can easy transform to SOCP constraint as (11c). Then, we have the standard SOCP constraint as follows:

$$\frac{\widetilde{p}_\ell^H\sqrt{|\boldsymbol{v}_\ell^\dagger\boldsymbol{g}_\ell|^2}}{\sqrt{\gamma_\ell^H}}\geq\sqrt{\sum_{j\neq\ell}^{L}(\widetilde{p}_j^H)^2|\boldsymbol{v}_\ell^\dagger\boldsymbol{g}_j|^2+\sum_{k=1}^{K}|\boldsymbol{v}_\ell^\dagger\boldsymbol{G}\boldsymbol{w}_k|^2+(\widetilde{\sigma}_\ell^{\mathrm{H}})^2}. \tag{30}$$

Then, we fix $\{\boldsymbol{w}_k\}$ and $\{p_\ell^H\}$. The optimal $\{\boldsymbol{v}_\ell\}$ is the MMSE solver (10).

3) Constraint (26d): Although (26d) cannot be directly converted to conic constraint, we can use the same structure as (27). In other words, (26d) and (27) have the same term on different signs, i.e., $\sum_{i\neq k}^{K}|\boldsymbol{h}_k^\dagger\boldsymbol{w}_i|^2+\sum_{\ell=1}^{L}|h_{k,\ell}|^2(\widetilde{p}_\ell^H)^2$. Therefore, (26d) can be expressed as

$$(1+\frac{1}{\gamma_k^M})|\boldsymbol{h}_k^\dagger\boldsymbol{w}_k|^2\geq\frac{E_k^M}{\beta_k^2}+r_k^2. \tag{31}$$

Also, we introduce another auxiliary variable $q_k>0\ \forall k$ such that $q_k^2=(E_k^M/\beta_k^2)$, and utilizing (29), (31) can convert into the form of the SOCP constraints

$$\sqrt{q_k^2+r_k^2}\leq\sqrt{1+\frac{1}{\gamma_k^M}}\boldsymbol{h}_k^\dagger\boldsymbol{w}_k, \tag{32a}$$

$$\sqrt{(q_k-\beta_k)^2+4\sqrt{E_k^M}}\leq q_k+\beta_k. \tag{32b}$$

The SOCP form is given by

$$\min_{\substack{\{\boldsymbol{w}_k\},\{\widetilde{p}_\ell^H\},\\ \{\alpha_k\},\{\beta_k\},\{r_k\},\{q_k\}}}\ \sum_{k=1}^{K}\|\boldsymbol{w}_k\|^2+\sum_{\ell=1}^{L}(\widetilde{p}_\ell^H)^2 \tag{33a}$$

$$\text{s.t.}\ \sqrt{\sum_{i\neq k}^{K}|\boldsymbol{h}_k^\dagger\boldsymbol{w}_i|^2+\sum_{\ell=1}^{L}|h_{k,\ell}|^2(\widetilde{p}_\ell^H)^2+(\sigma_k^{\mathrm{M}})^2+r_k^2}\leq\frac{\boldsymbol{h}_k^\dagger\boldsymbol{w}_k}{\sqrt{\gamma_k^M}}\ \forall k \tag{33b}$$

$$\sqrt{\sum_{j\neq\ell}^{L}(\widetilde{p}_j^H)^2|\boldsymbol{v}_\ell^\dagger\boldsymbol{g}_j|^2+\sum_{k=1}^{K}|\boldsymbol{v}_\ell^\dagger\boldsymbol{G}\boldsymbol{w}_k|^2+(\widetilde{\sigma}_\ell^{\mathrm{H}})^2}\leq\frac{\widetilde{p}_\ell^H\sqrt{|\boldsymbol{v}_\ell^\dagger\boldsymbol{g}_\ell|^2}}{\sqrt{\gamma_\ell^H}}\ \forall\ell \tag{33c}$$

$$\sqrt{q_k^2+r_k^2}\leq\sqrt{1+\frac{1}{\gamma_k^M}}\boldsymbol{h}_k^\dagger\boldsymbol{w}_k\ \forall k \tag{33d}$$

$$\sqrt{(r_k-\alpha_k)^2+4\widetilde{\sigma}_k}\leq r_k+\alpha_k\ \forall k \tag{33e}$$

$$\sqrt{(q_k-\beta_k)^2+4\sqrt{E_k^M}}\leq q_k+\beta_k\ \forall k \tag{33f}$$

$$\sqrt{\alpha_k^2+\beta_k^2}\leq 1,\ \ r_k\geq 0,\ \ q_k\geq 0\ \forall k \tag{33g}$$

$$\mathrm{Re}(\boldsymbol{h}_k^\dagger\boldsymbol{w}_k)\geq 0\ \forall k \tag{33h}$$

$$\mathrm{Im}(\boldsymbol{h}_k^\dagger\boldsymbol{w}_k)=0\ \forall k. \tag{33i}$$

Algorithm 2 MMSE-SOCP Relaxation AO Algorithm for Problem (8): Low-Complexity Optimal Design

Initialization: Given UL beamforming $\{\boldsymbol{v}_\ell^{(0)}\}\ \forall\ell$; set $t\leftarrow 0$.
repeat
  Obtain $\{\boldsymbol{w}_k^{(t)},\widetilde{p}_\ell^{\mathrm{H(t)}},\alpha_k^{(t)},\beta_k^{(t)},r_k^{(t)},q_k^{(t)}\}$ by solving problem (33).
  Given $\{\boldsymbol{w}_k^{(t)},\widetilde{p}_\ell^{\mathrm{H(t)}}\}$, obtain the UL beamforming $\{\boldsymbol{v}_\ell^{(t+1)}\}$.
  $t\leftarrow t+1$
until (34) is satisfied.

We propose the MMSE-SOCP relaxation iterative algorithm for solving problem (8). First, the receive beamforming $\{\boldsymbol{v}_\ell\}$ of (33) is fixed, i.e., MMSE. Thus, the relaxed SOCP problem (33) is a convex problem. By convex optimization tools (CVX) [35], we have $\{\boldsymbol{w}_k\},\{\widetilde{p}_\ell^H\},\{\alpha_k\},\{\beta_k\},\{r_k\},\{q_k\}$. Next, we can obtain the MMSE solution $\{\boldsymbol{v}_\ell\}$ in (10). Algorithm 2 summarizes the MMSE-SOCP relaxation algorithm. The procedure of Algorithm 2 is alternated. In Algorithm 2, the stopping criterion is given by

$$\text{The stopping criterion}=\frac{|\mathrm{C}_{\mathrm{opt}}^{\star\ (t+1)}-\mathrm{C}_{\mathrm{opt}}^{\star\ (t)}|}{\mathrm{C}_{\mathrm{opt}}^{\star\ (t)}}<\epsilon_3 \tag{34}$$

where $\mathrm{C}_{\mathrm{opt}}^{\star\ (t+1)}$ and $\mathrm{C}_{\mathrm{opt}}^{\star\ (t)}$ represent the optimal values of (33) at the $(t+1)$th and tth iteration results, respectively. The stopping criterion is ϵ_3.

It is worth noting that Algorithm 2 will converge to the KKT solution, similar to [42], [48, Lemma 4]. The key is that there is no phase rotation in the SOCP problem (33) [38], [42]. The following theorem shows the convergence and optimality of Algorithm 2.

Theorem 5: Suppose that problem (33) is feasible given initial values $\{\boldsymbol{v}_\ell^{(0)}\}\ \forall\ell$. In Algorithm 2, the objective function $\sum_{k=1}^{K}\|\boldsymbol{w}_k^{(t)}\|^2+\sum_{\ell=1}^{L}((\widetilde{p}_\ell^H)^{(t)})^2$ is nonincreasing with the iteration number t and the algorithm converges to a limit point as $t\to\infty$. Moreover, any limit point of Algorithm 2 is a KKT point.

Proof: See Appendix D. ■

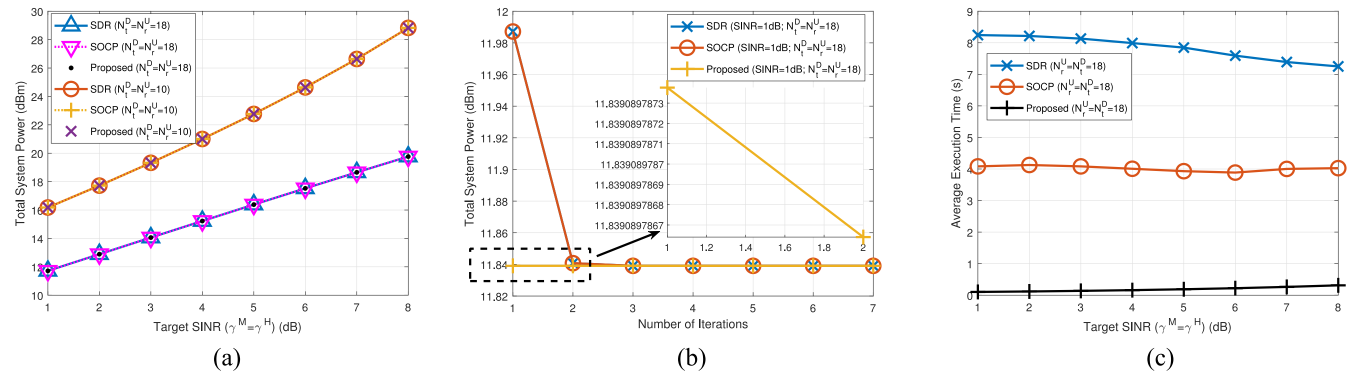

Fig. 3. JBPA: (a) Power versus SINR ($\gamma_k^M = \gamma_\ell^H$), (b) convergence behaviors of the proposed UDD algorithm, with target SINR = 1 dB, and $N_t^D = N_r^U = 18$, and (c) computational time versus SINR ($\gamma_k^M = \gamma_\ell^H$), with $K = 10$ and $L = 6$. In (c), computational time of the proposed UDD algorithm (Algorithm 1) are 0.1039, 0.1187, 0.1376, 0.1606, 0.1886, 0.2220, 0.2632, and 0.3129, from left to right.

C. Computational Complexity

Following a similar analysis as in Section IV-D, we obtain the complexity results as follows. For the SDR-based AO method (JBPAEH), the computational complexity is calculated by

$$\sqrt{(3K+L)}\mathcal{O}\Big(I\Big((2K+1)(N_t^D)^3 + L(N_r^U)^3\Big)\Big). \quad (35)$$

For the SOCP relaxation-based AO method (JBPAEH), the computational complexity is calculated by

$$\sqrt{(5K+L)}\cdot \mathcal{O}\Big(I\Big((5K+1)(N_t^D)^2 + L(N_r^U)^2 + L(N_r^U)^3\Big)\Big). \quad (36)$$

VI. Simulations Results

We simulate the two-cell network with parameter settings following from some standard approaches [33], [49]. The path loss model [49] between the DL BS and MTD channel is given by -145.4–$37.5\log_{10}(R)$ dB (The same path loss model used between the HTD and UL BS channel). The path loss model between the HTD and MTD channel is given by -175.78–$40\log_{10}(R)$ dB. Similarly, the path loss between the DL BS and UL BS channel is given by -169.36–$40\log_{10}(R)$ dB. R is the corresponding distance in kilometers. The noise power is set to $(\sigma_\ell^{\mathrm{H}})^2 = (\sigma_k^{\mathrm{M}})^2 = -70$ dBm because of the high bandwidth in 5G/6G wireless communication requirements [33]. The stopping criterion is set to $\epsilon_1 = \epsilon_2 = 10^{-8}$ for the precision in the algorithm. In every simulation results, the number of averaging is least 100 Rayleigh channel realizations. Moreover, in order to avoid infeasible issue in CVX [35] with high probability, we use the zero forcing (ZF) method to be the initial value, i.e., $\boldsymbol{v}_\ell^{(0)} = \widetilde{\boldsymbol{G}}^{-1}e_\ell$, where $\widetilde{\boldsymbol{G}} = [\boldsymbol{g}_1, \ldots, \boldsymbol{g}_L]^\top$ and e_ℓ is the standard unit vector [1]. The simulation results were implemented by using MATLAB on a desktop computer with Intel Core i7-8700 CPU @ 3.20 GHz. If not explicitly mentioned, we use these parameters throughout this article.

A. JBPA Optimization Problem

For the JBPA problem, we compare the SDR, SOCP, and the proposed Algorithm 1. We consider $L = 6$ HTDs and $K = 10$ MTDs, distributed according to the Poisson point process (PPP) with density $\bar{\lambda}^H = 8$ and $\bar{\lambda}^M = 9$, respectively. In Fig. 3, we present the same SINR requirement (threshold) performance, i.e., SINR $=$ SINR$_k^M$ $=$ SINR$_\ell^H$. In Fig. 3(a), we show the total system power versus target SINR. It is observed that the performance of SDR, SOCP, and the proposed algorithm (UDD). Interestingly, the performance of the proposed algorithm achieved the same result as SDR and SOCP. We can see that the total system power decreases since the number of antennas of BS increases (DL/UL BS). This is because there are fewer power requirements at the same SINR. It can also be observed from (6). In Fig. 3(b), we illustrate the convergence behaviors of the proposed algorithms with target SINR$_k^M$ $=$ SINR$_\ell^H$ $= 1$ dB. It can be observed that the proposed algorithm converges in two steps. Algorithm 1 almost converges immediately because we calculate the power and direction of the dual problem (13) in steps 2–6 of Algorithm 1. In other words, the fixed point functions are derived in the dual problem in Algorithm 1 so that Algorithm 1 converges faster than SDR and SOCP. In Fig. 3(c), we compare the computational complexity versus the SINR performance via average execution time. We can see that the proposed UDD method has faster computational time than the state-of-the-art SDR and SOCP.

In Fig. 4, we investigate the performance with different QoS settings. Specifically, the target SINR of HTD γ_ℓ^H varies from 1 to 8 dB, while the target SINR of MTD is fixed as $\gamma_k^M = 3$ dB. As expected, one can see that the optimal powers achieved by all the algorithms (i.e., SDR, SOCP, and the proposed UDD) are consistently the same, as shown in Fig. 4(a). As SDR/SOCP solutions are obtained from the seminal off-the-shelf CVX solver, such consistency demonstrates that the proposed UDD algorithm still works well even with nonuniform SINRs. Moreover, consider a specific instance of $(\gamma_k^M, \gamma_\ell^H) = (3, 1)$ dB and $N_t^D = N_r^U = 10$, we also show that the proposed UDD has fastest convergence rate, though SDR/SOCP also converge to same optimal values, as depicted in Fig. 4(b). In Fig. 4(c), one can see that the computational time of the proposed UDD algorithm is significantly faster.

Next, we investigate the performance of the proposed algorithms as the number of users increases, where the users are

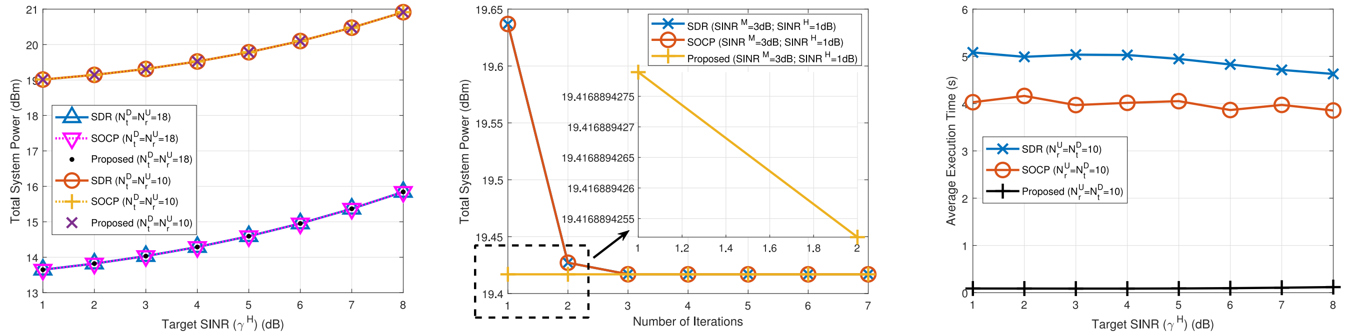

(a) (b) (c)

Fig. 4. JBPA: (a) Power versus SINR of HTD γ_ℓ^H (with SINR of MTD fixed at $\gamma_k^M = 3$ dB), (b) convergence behaviors of the proposed UDD algorithm when $(\gamma_k^M, \gamma_\ell^H) = (3, 1)$ dB and $N_t^D = N_r^U = 10$, and (c) computational time versus SINR (γ_ℓ^H) with $(K, L) = (10, 6)$, where the computational time of the proposed UDD algorithm (i.e., Algorithm 1) are 0.0887, 0.0877, 0.0867, 0.0868, 0.0893, 0.0957, 0.1060, and 0.1184 (s), from left to right.

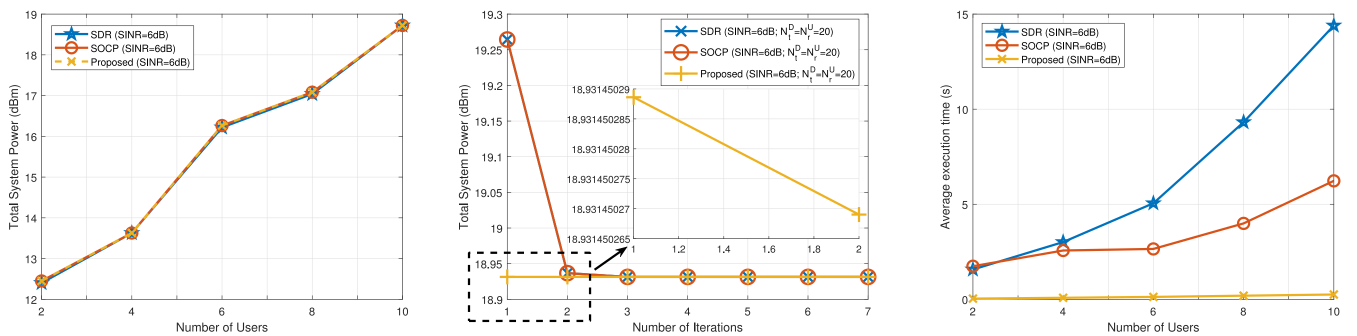

(a) (b) (c)

Fig. 5. JBPA: (a) Power versus the number of users $K = L \in \{2, 4, 6, 8, 10\}$, (b) convergence behaviors of the proposed UDD algorithm, with target $\gamma_k^M = \gamma_\ell^H = 6$ dB, and $N_t^D = N_r^U = 20$, and (c) computational time of the proposed UDD algorithm with $N_t^D = N_r^U = 20$.

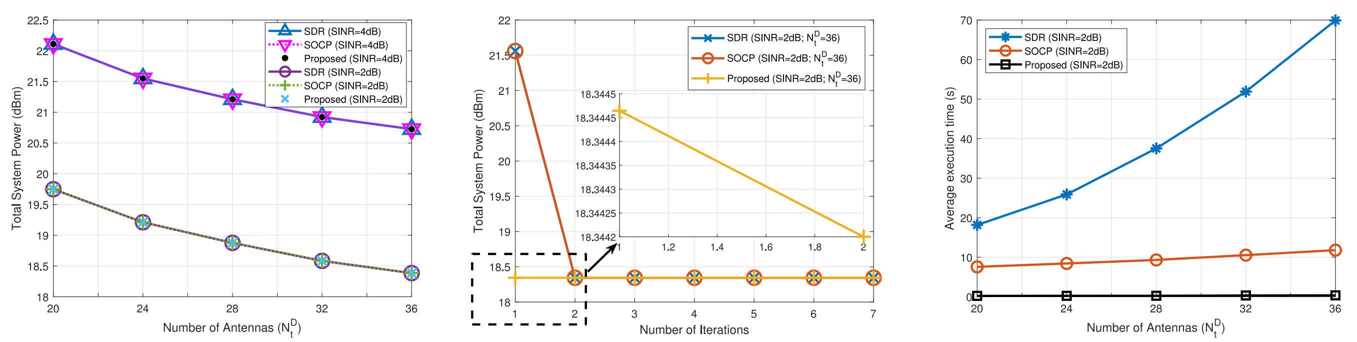

(a) (b) (c)

Fig. 6. JBPA: (a) Power versus the number of antennas (N_t^D), (b) convergence behaviors of the proposed UDD algorithm, with target $\gamma_k^M = \gamma_\ell^H = 2$ dB, and $N_r^U = 20$, and (c) computational time of the proposed UDD algorithm (Algorithm 1) are 0.2259, 0.2379, 0.2555, 0.3326, and 0.3606, from left to right.

uniformly distributed in two cells [50]. For both HTD/MTD user types, the number of users $(K = L)$ in each cell increases from 2 to 10. The parameter settings are $\gamma_k^M = \gamma_\ell^H = 6$ dB and $N_t^D = N_r^U = 20$. The radii of both UL/DL BSs are 40 m. As expected, the system power increases when the number of users increases as shown in Fig. 5(a), where one again confirms that the proposed UDD (i.e., Algorithm 1) converges to the same global optimal as SDR/SOCP solutions. In Fig. 5(b), UDD shows faster convergence rate. In Fig. 5(c), the computational time does increases when the number of users increases, comparing to which the computational time almost remains unaltered for different QoS settings. This result well matches our complexity analysis result (22), which depends on K, L but is independent of $(\gamma_k^M, \gamma_\ell^H)$; cf. Section IV-D for further details.

In Fig. 6, we evaluate the power versus the number of antennas at DL BS (N_t^D). In this simulation, we observe different topologies (PPP) to verify the efficiency of our method. The number of MTDs and HTDs are $K = 9$ $(\bar{\lambda}^M = 11)$ and $L = 12$ $(\bar{\lambda}^H = 12)$, respectively. The number of UL antennas is set to $N_r^U = 20$. In Fig. 6(a), when the number of DL antennas increases from 20 to 36, the total system power decreases.

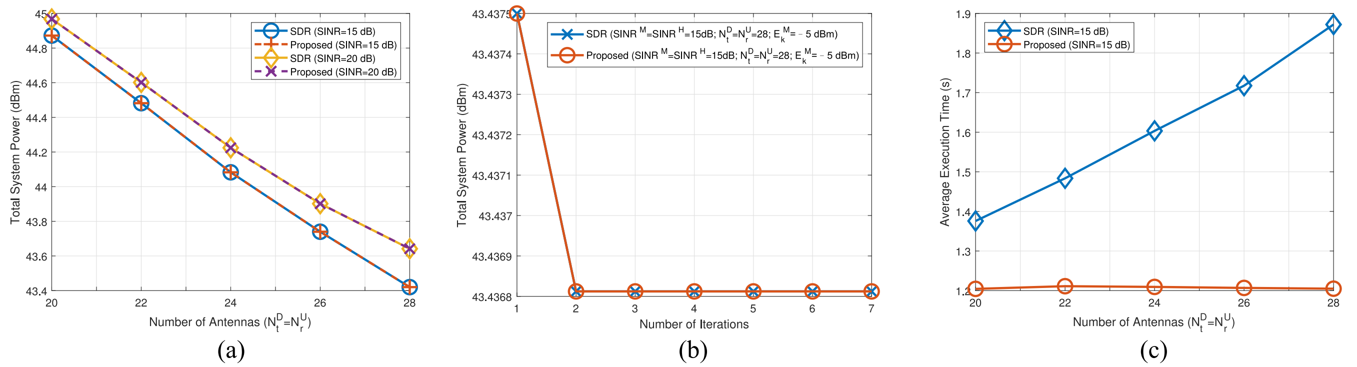

Fig. 7. JBPAEH: (a) Power versus the number of antennas ($N_t^D = N_r^U$), (b) convergence behaviors of the proposed SOCP relaxation algorithm, with target $\gamma_k^M = \gamma_\ell^H = 15$ dB, and $N_t^D = N_r^U = 28$, and (c) computational time of the proposed SOCP relaxation algorithm ($N_t^D = N_r^U$), with $E_k^M = -5$ dBm, $K = 2$, and $L = 2$.

TABLE II
JBPAEH: SINR ($\gamma = \gamma_k^M = \gamma_\ell^H$), Optimal PS Ratio ($\rho_k$), and Target EH Requirement (E_k^M), Where $k = 1$, and $N_r^U = N_t^D = 28$

ρ_k \ E_k^{M} / γ	$E_k^{\mathrm{M}} = -25$ dBm	$E_k^{\mathrm{M}} = -20$ dBm	$E_k^{\mathrm{M}} = -15$ dBm	$E_k^{\mathrm{M}} = -10$ dBm	$E_k^{\mathrm{M}} = -5$ dBm	$E_k^{\mathrm{M}} = 0$ dBm
$\gamma = 15$ dB	$\rho_k = [0.0944]$	$\rho_k = [0.0366]$	$\rho_k = [0.0183]$	$\rho_k = [0.0101]$	$\rho_k = [0.0057]$	$\rho_k = [0.0032]$
$\gamma = 20$ dB	$\rho_k = [0.2411]$	$\rho_k = [0.0922]$	$\rho_k = [0.0334]$	$\rho_k = [0.0135]$	$\rho_k = [0.0067]$	$\rho_k = [0.0036]$

We also can see that when the SINR requirement increases, the power consumption in the y-axis increases, as discussed previously. Also, we evaluate the convergence behaviors of the proposed UDD algorithm in Fig. 6(b). In Fig. 6(c), we also compare the computational time versus the number of antennas at the DL BS performance. The proposed UDD algorithm has fast computational time than SDR and SOCP.

B. JBPAEH Optimization Problem

For the JBPAEH problem, we compare the SDR and the proposed Algorithm 2. Note that (25) and (33) are complicated convex problems, and it is not easy to find a feasible solution set for both (25) and (33) simultaneously. Thus, similar to [48], [50], and [51], we consider a simplified scenario with uniformly distributed $L = 2$ HTDs and $K = 2$ MTDs. We set the variances of the circuit noises to $\widetilde{\sigma}_k^2 = -50$ dBm [45], [52]. Algorithm 2 is stopped by $\epsilon_3 = 10^{-2}$. Table II shows the relationship between SINRs ($\gamma = \gamma_k^M = \gamma_\ell^H$, in dB), EH requirements (E_k^M, in dBm), and PS ratios (ρ_k), where ρ_k has no measurement unit. We set $N_r^U = N_t^D = 28$ and display the performances for an arbitrary MTD (i.e., the first MTD, where $k = 1$), as same results are obtained for all other MTDs. We can observe that when EH requirement (E_k^M) adds, the PS factor (ρ_k) decreases. The reason is that more energy is required for the EH circuit of the receiving MTD to achieve the higher requirement. Similarly, when SINR ($\gamma = \gamma_k^M = \gamma_\ell^H$) increases, the PS factor (ρ_k) increases, because more energy is required to meet the ID requirement of the MTD to achieve the higher target QoS. This well-known tradeoff between the ID requirement and EH can be referred to [13] and [14].

Fig. 7 shows the power versus the number of antennas at DL/UL BS ($N_t^D = N_r^U$). It can be observed that the power decreases from left to right with an increasing number of antennas at DL/UL BS in Fig. 7(a). It is easy to check from (6) and (8), i.e., when we increase the number of antennas at DL/UL BS, SINR in (6) and (8) need less power in $\{\boldsymbol{p}_\ell^H\}$ to achieve the same SINR requirement. Due to the hard coupled problem of (33), we also examine the `cvx` in MATLAB, e.g., **`CVX solver: SeDuMi`** and **`CVX precision`**, etc. Fig. 7(b) compares the convergence behaviors of the proposed SOCP relaxation algorithm. The convergence of the SOCP relaxation is in two step. In Fig. 7(c), we compare the computational time versus the number of antennas at DL/UL BS. The proposed algorithm has faster computational time than SDR since the computational effort required for matrix operations in SDR is more than that for vector operations in the proposed SOCP relaxation-based method.

VII. Conclusion and Future Work

Finally, we present the conclusion of this article and the future work for the coexistence issue in IoT development.

A. Conclusion

We have considered JBPA and JBPAEH for M2M/H2H coexistence with dynamic green TDD system in this work. The design objective is QoS-constrained power minimization in JBPA and QoS as well as EH-constrained power minimization in JBPAEH. First, we investigated a simplified problem where each device is assumed having no EH capabilities. In the simplified problem, the resulting optimization problem is challenging to solve because the design variables are tightly coupled in the constraints. We proposed a novel low-complexity UDD-based AO algorithm to solve the problem. Then, we proposed a low-complexity SOCP relaxation-based AO algorithm to deal with the tightly coupled problem with EH considerations. Numerical results demonstrated the performance of the proposed UDD and SOCP relaxation algorithm from different perspectives.

B. Future Work

In the future 6G research direction, we will consider the intelligent reflecting surface (IRS) and machine learning (ML) to assist the H2H/M2M coexistence issue in green dynamic TDD [53]–[55]. By IRS-assisted EH in dynamic TDD scenario, the cross-link interference control and EH requirements are more "intelligent" management. In addition, extending the current formulation for accounting the scenario with massive machine-type communications (M2M/H2H coexistence) is an interesting future research line, which would be handled by the popular *Q*-learning in reinforcement learning [53] and by fast UL/DL beamforming design via deep learning [55]. Finally, investigating the multicell dynamic TDD design for H2H/M2M coexistence issue under the additional EH constraints should also be a challenging research direction deserving more attentions. Moreover, JBPA design of D2D communication in H2H/M2M coexistence is also a challenging work in the future.

Appendix A
Proof of Theorem 1

Due to the convexity of (9), Slater's condition is satisfied, i.e., the duality gap is zero [47]. The Lagrangian of the problem (9) is given by

$$\begin{aligned}\mathcal{L}(\boldsymbol{W},\boldsymbol{p}^H,\boldsymbol{\lambda}^M,\boldsymbol{\lambda}^H,\boldsymbol{A}) &= \sum_{k=1}^{K}\mathrm{Tr}(\boldsymbol{W}_k)+\sum_{\ell=1}^{L}p_\ell^H\\ &-\sum_{k=1}^{K}\lambda_k^M\left(\frac{\boldsymbol{h}_k^\dagger\boldsymbol{W}_k\boldsymbol{h}_k}{\gamma_k^M}-\sum_{i\neq k}^{K}\boldsymbol{h}_k^\dagger\boldsymbol{W}_i\boldsymbol{h}_k-\sum_{\ell=1}^{L}|h_{k,\ell}|^2p_\ell^H\right.\\ &\left.-(\sigma_k^{\mathrm{M}})^2\right)-\sum_{\ell=1}^{L}\lambda_\ell^H\left(\frac{p_\ell^H|\boldsymbol{v}_\ell^\dagger\boldsymbol{g}_\ell|^2}{\gamma_\ell^H}-\sum_{j\neq\ell}^{L}p_j^H|\boldsymbol{v}_\ell^\dagger\boldsymbol{g}_j|^2-\sum_{k=1}^{K}\xi_{\ell,k}\right.\\ &\left.-(\widetilde{\sigma}_\ell^{\mathrm{H}})^2\right)-\sum_{k=1}^{K}\mathrm{Tr}(\boldsymbol{A}_k\boldsymbol{W}_k) \end{aligned}\tag{37}$$

where $\boldsymbol{W}=[\boldsymbol{w}_1,\ldots,\boldsymbol{w}_K]$; $\boldsymbol{p}^H,\boldsymbol{\lambda}^M$, and $\boldsymbol{\lambda}^H$ are denoted in (14). $\boldsymbol{A}$ is the Lagrange multiplier of semidefinite constraint. Rearranging the terms of (37), we have

$$\begin{aligned}\mathcal{L}(\boldsymbol{W},\boldsymbol{p}^H,\boldsymbol{\lambda}^M,\boldsymbol{\lambda}^H,\boldsymbol{A}) &= \sum_{k=1}^{K}\mathrm{Tr}\left\{\left(\boldsymbol{I}_{N_t^D}+\sum_{i\neq k}^{K}\lambda_i^M\boldsymbol{h}_i\boldsymbol{h}_i^\dagger\right.\right.\\ &\left.\left.+\sum_{\ell=1}^{L}\lambda_\ell^H\boldsymbol{G}^\dagger\boldsymbol{v}_\ell\boldsymbol{v}_\ell^\dagger\boldsymbol{G}-\lambda_k^M\frac{\boldsymbol{h}_k\boldsymbol{h}_k^\dagger}{\gamma_k^M}-\boldsymbol{A}_k\right)\boldsymbol{W}_k\right\}+\sum_{\ell=1}^{L}p_\ell^H\\ &+\sum_{k=1}^{K}\lambda_k^M\left(\sum_{\ell=1}^{L}|h_{k,\ell}|^2p_\ell^H+(\sigma_k^{\mathrm{M}})^2\right)\\ &-\sum_{\ell=1}^{L}\lambda_\ell^H\left(\frac{p_\ell^H|\boldsymbol{v}_\ell^\dagger\boldsymbol{g}_\ell|^2}{\gamma_\ell^H}-\sum_{j\neq\ell}^{L}p_j^H|\boldsymbol{v}_\ell^\dagger\boldsymbol{g}_j|^2-(\widetilde{\sigma}_\ell^{\mathrm{H}})^2\right). \end{aligned}\tag{38}$$

The corresponding KKT conditions are given by

$$\frac{\partial\mathcal{L}(\boldsymbol{W},\boldsymbol{p}^H,\boldsymbol{\lambda}^M,\boldsymbol{\lambda}^H,\boldsymbol{A})}{\partial\boldsymbol{W}_k}=0\ \forall k \tag{39a}$$

$$\boldsymbol{A}_k\boldsymbol{W}_k=0\ \forall k \tag{39b}$$

$$\boldsymbol{A}_k\succeq 0,\ \boldsymbol{W}_k\succeq 0,\ \lambda_k^M\geq 0\ \forall k \tag{39c}$$

$$\lambda_\ell^H\geq 0\ \forall\ell. \tag{39d}$$

From (39a), we have

$$\boldsymbol{A}_k=\underbrace{\boldsymbol{I}_{N_t^D}+\sum_{i\neq k}^{K}\lambda_i^M\boldsymbol{h}_i\boldsymbol{h}_i^\dagger+\sum_{\ell=1}^{L}\lambda_\ell^H\boldsymbol{G}^\dagger\boldsymbol{v}_\ell\boldsymbol{v}_\ell^\dagger\boldsymbol{G}}_{\boldsymbol{B}_k}-\lambda_k^M\frac{\boldsymbol{h}_k\boldsymbol{h}_k^\dagger}{\gamma_k^M}. \tag{40}$$

Let $\{(\lambda_k^M)^*\}$, and $\{(\lambda_\ell^H)^*\}$ denote the optimal dual solution to problem (9). Correspondingly, let $\boldsymbol{A}_k^*=\boldsymbol{A}_k((\lambda_k^M)^*,(\lambda_\ell^H)^*)$.

If $\boldsymbol{B}_k^*$ is positive definite, Rank($\boldsymbol{B}_k^*$) $=N_t^D$ and Rank($\boldsymbol{A}_k^*$) $\geq N_t^D-1$. However, if Rank($\boldsymbol{A}_k^*$) $=N_t^D$, i.e., $\boldsymbol{A}_k^*$ is full rank, then it follows from (39b) that $\boldsymbol{W}_k^*=0$, which cannot be an optimal solution to (9). Moreover, in order to satisfy the SINR constraints, it must hold $\boldsymbol{W}_k^*\neq 0\ \forall k$. Furthermore, in order to avoid an unbounded below, it must follow $\boldsymbol{A}_k^*\succeq 0$. Hence, the complementary slackness $\boldsymbol{A}_k^*\boldsymbol{W}_k^*=0$ in the KKT condition should satisfy. According to $\boldsymbol{A}_k^*\succeq 0$ and $\boldsymbol{W}_k^*\succ 0$, we have $\boldsymbol{A}_k^*\boldsymbol{W}_k^*=0$. From (40), it is evident that $\boldsymbol{A}_k^*$ has at most one zero eigenvalue, and therefore, Rank($\boldsymbol{A}_k^*$) $\geq N_t^D-1\ \forall k$ [33], [46]. Then, according to the complementary slackness of the KKT condition $\boldsymbol{A}_k^*\boldsymbol{W}_k^*=0$, Rank($\boldsymbol{W}_k^*$) $=1$ when the problem is feasible. Thus, the key is to show that $\boldsymbol{B}_k^*\succ 0$, i.e., Rank($\boldsymbol{B}_k^*$) $=N_t^D$.

Due to $\boldsymbol{A}_k^*\succeq 0$ and $-(\lambda_k^M)^*(\boldsymbol{h}_k\boldsymbol{h}_k^\dagger/\gamma_k^M)\preceq 0$, we have $\boldsymbol{B}_k^*\succeq 0$. In the subsequent, we show that $\boldsymbol{B}_k^*\succ 0$ by contradiction. Assume $\boldsymbol{B}_k^*$ has the minimum eigenvalue zero. Therefore, there exists at least an $z\neq\mathbf{0}$ such that $z^\dagger\boldsymbol{B}_k^*z=0$. According to (40), it follows that:

$$z^\dagger\boldsymbol{A}_k^*z=-\frac{(\lambda_k^M)^*}{\gamma_k^M}z^\dagger\boldsymbol{h}_k\boldsymbol{h}_k^\dagger z=-\frac{(\lambda_k^M)^*}{\gamma_k^M}|z^\dagger\boldsymbol{h}_k|^2. \tag{41}$$

Since $\lambda_k^M>0$, we have $z^\dagger\boldsymbol{A}_k^*z\leq 0$. This implies that $\boldsymbol{A}_k^*$ is a negative semidefinite, which in turn violates the KKT condition. Therefore, $\boldsymbol{B}_k^*\succ 0$ must hold. In other words, $\boldsymbol{W}_k^*\ \forall k$ must lie in the null space of $\boldsymbol{A}_k^*\ \forall k$ whose dimension is one. Thus, the optimal $\boldsymbol{W}_k^*\ \forall k$ to (9) is rank one.

Appendix B
Proof of Theorem 3

We will prove three properties of fixed point, i.e., positivity, monotonicity, and scalability. The proofs are based on the following lemma [37, Proposition 4].

Lemma 1: If $\boldsymbol{A}\succeq 0$, $\boldsymbol{B}\succeq 0$ and $\mathbf{c}$ is in the range of $\boldsymbol{A}$, then

$$\frac{1}{\mathbf{c}^\dagger(\boldsymbol{A}+\boldsymbol{B})^{-1}\mathbf{c}}\geq\frac{1}{\mathbf{c}^\dagger\boldsymbol{A}^{-1}\mathbf{c}} \tag{42}$$

with equality if and only if $\boldsymbol{B}(\boldsymbol{A}+\boldsymbol{B})^{-1}\mathbf{c}=0$.

According to [37, Proposition 4], we can show that the unique fixed-point iteration of (18) obeys the following three properties.

1) *Positivity:* The positivity can be easily seen since the transmit power is always non-negative.

2) *Monotonicity:* The virtual HTD part $\mathcal{F}_\ell^H(\boldsymbol{\lambda}^M, \boldsymbol{\lambda}^H) > \mathcal{F}_\ell^H((\boldsymbol{\lambda}^M)', (\boldsymbol{\lambda}^H)')\ \forall \ell$ is obvious. The virtual MTD part is as follows:

$$\begin{aligned}
&\mathcal{F}_k^M(\boldsymbol{\lambda}^M, \boldsymbol{\lambda}^H)\\
&= \frac{1}{\boldsymbol{h}_k^\dagger\left(\sum_{i=1}^K \lambda_i^M \boldsymbol{h}_i\boldsymbol{h}_i^\dagger + \sum_{\ell=1}^L \lambda_\ell^H \widetilde{\boldsymbol{G}} + \boldsymbol{I}\right)^{-1}\boldsymbol{h}_k \xi_k^M}\\
&= \frac{1}{\boldsymbol{h}_k^\dagger\left(\sum_{i=1}^K \lambda_i^M \boldsymbol{h}_i\boldsymbol{h}_i^\dagger + \sum_{\ell=1}^L \lambda_\ell^H \widetilde{\boldsymbol{G}} + \boldsymbol{I} + \Gamma\right)^{-1}\boldsymbol{h}_k \xi_k^M}\\
&\geq \frac{1}{\boldsymbol{h}_k^\dagger\left(\sum_{i=1}^K (\lambda_i^M)' \boldsymbol{h}_i\boldsymbol{h}_i^\dagger + \sum_{\ell=1}^L (\lambda_\ell^H)' \widetilde{\boldsymbol{G}} + \boldsymbol{I}\right)^{-1}\boldsymbol{h}_k \xi_k^M}\\
&= \mathcal{F}_k^M((\boldsymbol{\lambda}^M)', (\boldsymbol{\lambda}^H)')\ \forall k, \qquad (43)
\end{aligned}$$

where $\widetilde{\boldsymbol{G}} = \boldsymbol{G}^\dagger \boldsymbol{v}_\ell \boldsymbol{v}_\ell^\dagger \boldsymbol{G}$, $\xi_k^M = (1 + [1/\gamma_k^M])$, and $\Gamma = \sum_{i=1}^K (\lambda_i^M)' \boldsymbol{h}_i\boldsymbol{h}_i^\dagger + \sum_{\ell=1}^L (\lambda_\ell^H)' \widetilde{\boldsymbol{G}} - \sum_{i=1}^K (\lambda_i^M)' \boldsymbol{h}_i\boldsymbol{h}_i^\dagger - \sum_{\ell=1}^L (\lambda_\ell^H)' \widetilde{\boldsymbol{G}}$.

3) *Scalability:* The virtual MTD part is as follows:

$$\begin{aligned}
&\alpha\mathcal{F}_k^M(\boldsymbol{\lambda}^M, \boldsymbol{\lambda}^H)\\
&= \frac{\alpha}{\boldsymbol{h}_k^\dagger\left(\sum_{i=1}^K \lambda_i^M \boldsymbol{h}_i\boldsymbol{h}_i^\dagger + \sum_{\ell=1}^L \lambda_\ell^H \widetilde{\boldsymbol{G}} + \boldsymbol{I}\right)^{-1}\boldsymbol{h}_k \xi_k^M}\\
&= \frac{1}{\boldsymbol{h}_k^\dagger\left(\sum_{i=1}^K \alpha\lambda_i^M \boldsymbol{h}_i\boldsymbol{h}_i^\dagger + \sum_{\ell=1}^L \alpha\lambda_\ell^H \widetilde{\boldsymbol{G}} + \widetilde{\alpha}\right)^{-1}\boldsymbol{h}_k \xi_k^M}\\
&\geq \frac{1}{\boldsymbol{h}_k^\dagger\left(\sum_{i=1}^K \alpha\lambda_i^M \boldsymbol{h}_i\boldsymbol{h}_i^\dagger + \sum_{\ell=1}^L \alpha\lambda_\ell^H \widetilde{\boldsymbol{G}} + \boldsymbol{I}\right)^{-1}\boldsymbol{h}_k \xi_k^M}\\
&= \mathcal{F}_k^M(\alpha\boldsymbol{\lambda}^M, \alpha\boldsymbol{\lambda}^H)\ \forall k \qquad (44)
\end{aligned}$$

where $\widetilde{\alpha} = \boldsymbol{I} + (\alpha - 1)\boldsymbol{I}$. The virtual HTD part is as follows:

$$\begin{aligned}
&\alpha\mathcal{F}_\ell^H(\boldsymbol{\lambda}^M, \boldsymbol{\lambda}^H)\\
&= \frac{\sum_{j=1}^L \alpha\lambda_j^H |\boldsymbol{v}_j^\dagger \boldsymbol{g}_\ell|^2 + \sum_{k=1}^K \alpha |h_{k,\ell}|^2 \lambda_k^M + \alpha}{|\boldsymbol{v}_\ell^\dagger \boldsymbol{g}_\ell|^2 (1 + \frac{1}{\gamma_\ell^H})}\\
&\geq \frac{\sum_{j=1}^L \alpha\lambda_j^H |\boldsymbol{v}_j^\dagger \boldsymbol{g}_\ell|^2 + \sum_{k=1}^K \alpha |h_{k,\ell}|^2 \lambda_k^M + 1}{|\boldsymbol{v}_\ell^\dagger \boldsymbol{g}_\ell|^2 (1 + \frac{1}{\gamma_\ell^H})}\\
&= \mathcal{F}_\ell^H(\alpha\boldsymbol{\lambda}^M, \alpha\boldsymbol{\lambda}^H)\ \forall \ell. \qquad (45)
\end{aligned}$$

Since problem (12) is an LP, the dual problem of (12) is also a convex problem [47]. Therefore, the UDD algorithm satisfies the Slater's condition and the duality gap is zero. In addition, the objective function $\sum_{k=1}^K \lambda_k^M (\sigma_k^{\mathrm{M}})^2 + \sum_{\ell=1}^L \lambda_\ell^H (\widetilde{\sigma}_\ell^{\mathrm{H}})^2$ of the problem (13) is nonincreasing (Max and Min are the same in the objective function [36], [42]). Moreover, any initial point of (18) will converge to an "unique" fixed point. Therefore, Algorithm 1 has optimality.

Appendix C
Proof of Theorem 4

Due to the convexity of (25), Slater's condition is satisfied [47]. The Lagrangian of the problem (25) is expressed as

$$\begin{aligned}
&\mathcal{L}(\boldsymbol{W}, \boldsymbol{p}^H, \boldsymbol{\rho}, \boldsymbol{\mu}^M, \boldsymbol{\mu}^H, \boldsymbol{\nu}^M) = \sum_{k=1}^K \mathrm{Tr}(\boldsymbol{W}_k) + \sum_{\ell=1}^L p_\ell^H\\
&- \sum_{k=1}^K \mu_k^M \Bigg(\frac{\boldsymbol{h}_k^\dagger \boldsymbol{W}_k \boldsymbol{h}_k}{\gamma_k^M} - \sum_{i\neq k}^K \boldsymbol{h}_k^\dagger \boldsymbol{W}_i \boldsymbol{h}_k - \sum_{\ell=1}^L |h_{k,\ell}|^2 p_\ell^H\\
&-(\sigma_k^{\mathrm{M}})^2 - \frac{\widetilde{\sigma}_k^2}{\rho_k}\Bigg) - \sum_{\ell=1}^L \mu_\ell^H \Bigg(\frac{p_\ell^H |\boldsymbol{v}_\ell^\dagger \boldsymbol{g}_\ell|^2}{\gamma_\ell^H} - \sum_{j\neq \ell}^L p_j^H |\boldsymbol{v}_\ell^\dagger \boldsymbol{g}_j|^2\\
&- \sum_{k=1}^K \boldsymbol{v}_\ell^\dagger \boldsymbol{G} \boldsymbol{W}_k \boldsymbol{G}^\dagger \boldsymbol{v}_\ell - (\widetilde{\sigma}_\ell^{\mathrm{H}})^2 \Bigg) - \sum_{k=1}^K \nu_k^M \Bigg(\sum_{i=1}^K \boldsymbol{h}_k^\dagger \boldsymbol{W}_i \boldsymbol{h}_k\\
&+ \sum_{\ell=1}^L |h_{k,\ell}|^2 p_\ell^H + (\sigma_k^{\mathrm{M}})^2 - \frac{E_k^M}{(1-\rho_k)} \Bigg). \qquad (46)
\end{aligned}$$

Thus, we have the Lagrangian dual problem of (25) as follows:

$$\min_{\substack{\{\boldsymbol{W}_k \succeq 0\}, \{\rho_k\},\\ \{p_\ell^H \geq 0\}}} \ \mathcal{L}(\boldsymbol{W}, \boldsymbol{p}^H, \boldsymbol{\rho}, \boldsymbol{\mu}^M, \boldsymbol{\mu}^H, \boldsymbol{\nu}^M) \qquad (47a)$$

$$\text{s.t. } 0 \leq \rho_k \leq 1\ \forall k \in \mathcal{K} \qquad (47b)$$

where the constraints (47b) are named box constraints or variable bounds [47, Sec. 5.7.3]. In (47a), the Lagrangian function can be explicitly rewritten as

$$\begin{aligned}
&\mathcal{L}(\boldsymbol{W}, \boldsymbol{p}^H, \boldsymbol{\rho}, \boldsymbol{\mu}^M, \boldsymbol{\mu}^H, \boldsymbol{\nu}^M) = \sum_{k=1}^K \mathrm{Tr}(\boldsymbol{A}_k \boldsymbol{W}_k) + \sum_{\ell=1}^L \mu_\ell^H (\widetilde{\sigma}_\ell^{\mathrm{H}})^2\\
&+ \sum_{k=1}^K \Bigg((\mu_k^M - \nu_k^M)(\sigma_k^{\mathrm{M}})^2 + \mu_k^M \frac{\widetilde{\sigma}_k^2}{\rho_k} + \nu_k^M \frac{E_k^M}{(1-\rho_k)} \Bigg)\\
&+ \sum_{\ell=1}^L (1 + \sum_{k=1}^K (\mu_k^M - \nu_k^M)|h_{k,\ell}|^2\\
&- \frac{|\boldsymbol{v}_\ell^\dagger \boldsymbol{g}_\ell|^2}{(\frac{1}{\mu_\ell^H})\gamma_\ell^H} + \sum_{j\neq \ell}^L \mu_j^H |\boldsymbol{v}_j^\dagger \boldsymbol{g}_\ell|^2) p_\ell^H
\end{aligned} \qquad (48)$$

where $\boldsymbol{A}_k = \boldsymbol{I}_{N_t^P} - ([\mu_k^M/\gamma_k^M] + \mu_k^M)\boldsymbol{h}_k\boldsymbol{h}_k^\dagger + \sum_{i=1}^K (\mu_i^M - \nu_i^M)\boldsymbol{h}_i\boldsymbol{h}_i^\dagger + \sum_{\ell=1}^L \mu_\ell^H \boldsymbol{G}^\dagger \boldsymbol{v}_\ell \boldsymbol{v}_\ell^\dagger \boldsymbol{G}$.

Let $\{(\mu_k^M)^*\}$, $\{(\mu_\ell^H)^*\}$, and $\{(\nu_k^M)^*\}$ denote the optimal dual solution to problem (25). Accordingly, we define $\boldsymbol{A}_k^* = \boldsymbol{A}_k((\mu_k^M)^*, (\mu_\ell^H)^*, (\nu_k^M)^*)$. Besides, in order to avoid an unbounded below, it must follow $\boldsymbol{A}_k^* \succeq 0$. Also, the optimal PS ratio ρ_k^* from (47) must be the optimal solution of the problem

$$\begin{aligned}
&\min_{\rho_k} \ \left(\sum_{k=1}^K (\mu_k^M)^* \frac{\widetilde{\sigma}_k^2}{\rho_k} + (\nu_k^M)^* \frac{E_k^M}{(1-\rho_k)} \right)\\
&\text{s.t. } 0 \leq \rho_k \leq 1\ \forall k \in \mathcal{K}. \qquad (49)
\end{aligned}$$

Next, we prove the above problem by discussing following three cases about $(\mu_k^M)^*$ and $(\nu_k^M)^*$. If $(\mu_k^M)^* > 0$ and $(\nu_k^M)^* =$

0, the optimal solution will be $\rho_k^* \to 1$. If $(\mu_k^M)^* = 0$ and $(\nu_k^M)^* > 0$, the optimal solution will be $\rho_k^* \to 0$. If $(\mu_k^M)^* = 0$ and $(\nu_k^M)^* = 0$, we will prove that this case cannot happen for any k by contradiction. Assume there exist some $k's$ such that $(\mu_k^M)^* = (\nu_k^M)^* = 0$. Let a set $\Psi \triangleq \{k|(\mu_k^M)^* = 0, (\nu_k^M)^* = 0, 1 \le k \le K\}$ and $\Psi \neq \emptyset$. Then, $\boldsymbol{A}_k^*$ can be rewritten as

$$\boldsymbol{A}_k^* = \begin{cases} \boldsymbol{B}_k^*, & k \in \Psi \\ \boldsymbol{B}_k^* - \left(\frac{\mu_k^M}{\gamma_k^M} + \mu_k^M\right)\boldsymbol{h}_k\boldsymbol{h}_k^\dagger, & k \notin \Psi \end{cases} \tag{50}$$

where $\boldsymbol{B}^* = \boldsymbol{I}_{N_t^D} + \sum_{i=1}^K (\mu_i^M - \nu_i^M)\boldsymbol{h}_i\boldsymbol{h}_i^\dagger + \sum_{\ell=1}^L \mu_\ell^H \boldsymbol{G}^\dagger \boldsymbol{v}_\ell \boldsymbol{v}_\ell^\dagger \boldsymbol{G}$. Due to $\boldsymbol{A}_k^* \succeq 0$ and $-([(\mu_k^M)^*/\gamma_k^M] + (\mu_k^M)^*)\boldsymbol{h}_k\boldsymbol{h}_k^\dagger \preceq 0$, we have $\boldsymbol{B}_k^* \succeq 0$. Next, we proof that $\boldsymbol{B}_k^* \succ 0$ by contradiction. Assume $\boldsymbol{B}_k^*$ has the eigenvalue zero. Thus, we have at least an $\boldsymbol{z} \neq \boldsymbol{0}$ such that $\boldsymbol{z}^\dagger \boldsymbol{B}_k^* \boldsymbol{z} = 0$. According to (50), we have that

$$\boldsymbol{z}^\dagger \boldsymbol{A}_k^* \boldsymbol{z} = -\left(\frac{(\mu_k^M)^*}{\gamma_k^M} + (\mu_k^M)^*\right)\boldsymbol{z}^\dagger \boldsymbol{h}_k \boldsymbol{h}_k^\dagger \boldsymbol{z},\ k \notin \Psi. \tag{51}$$

Note that we have $(\mu_k^M)^* > 0$ if $k \notin \Psi$. According to (51), we have $|\boldsymbol{h}_k^\dagger \boldsymbol{z}|^2 \le 0, k \notin \Psi$. It thus follows that $\boldsymbol{h}_k^\dagger \boldsymbol{z} = 0, k \notin \Psi$. Thus, we obtain $\boldsymbol{z}^\dagger \boldsymbol{B}^* \boldsymbol{z} = \boldsymbol{z}^\dagger \boldsymbol{z} + \sum_{\ell=1}^L \mu_\ell^H \boldsymbol{z}^\dagger \boldsymbol{G}^\dagger \boldsymbol{v}_\ell \boldsymbol{v}_\ell^\dagger \boldsymbol{G}\boldsymbol{z} > 0$. This contradicts to $\boldsymbol{z}^\dagger \boldsymbol{B}_k^* \boldsymbol{z} = 0$. Therefore, $\boldsymbol{B}_k^* \succ \boldsymbol{0}$, i.e., rank$(\boldsymbol{B}_k^*) = \boldsymbol{I}_{N_t^D}$. It follows from (50) that rank$(\boldsymbol{A}_k^*) = \boldsymbol{I}_{N_t^D}$ if $k \in \Psi$. On condition that the complementary slackness $\boldsymbol{A}_k^* \boldsymbol{W}_k^* = 0$ in the KKT condition, we have $\boldsymbol{W}_k^* = 0$ if $k \in \Psi$. However, if $\boldsymbol{A}_k^*$ is full rank (rank$(\boldsymbol{A}_k^*)$= N_t^D), then we have $\boldsymbol{W}_k^* = 0$ which cannot be an optimal beamforming solution to (25). Furthermore, in order to satisfy the SINR requirement constraints, it must hold $\boldsymbol{W}_k^* \neq 0\ \forall k$. Besides, in order to avoid an unbounded below, it must follow $\boldsymbol{A}_k^* \succeq 0$. Hence, we have rank$(\boldsymbol{A}_k^*)$= $N_t^D - 1$ and rank$(\boldsymbol{W}_k^*)$= 1. The optimal $\boldsymbol{W}_k^*\ \forall k$ to (25) is rank-one.

APPENDIX D
PROOF OF THEOREM 5

In problem (33), the objective function $\sum_{k=1}^K \|\boldsymbol{w}_k\|^2 + \sum_{\ell=1}^L (\widetilde{p}_\ell^H)^2$ is nonincreasing. Moreover, the problem is already transformed to an SOCP form. Assume $\boldsymbol{u}_k^*$ and $\boldsymbol{z}_k^*$ are any two optimal solutions to problem (8). Define $(\theta_k^{\boldsymbol{u}})^* \triangleq \angle(\boldsymbol{h}_k^\dagger \boldsymbol{u}_k^*)$ and $(\theta_k^{\boldsymbol{z}})^* \triangleq \angle(\boldsymbol{h}_k^\dagger \boldsymbol{z}_k^*)$ are the angle of $\boldsymbol{u}_k^*$ and the angle of $\boldsymbol{z}_k^*$, respectively. Analogous to [48, Lemma 4], we prove $\boldsymbol{u}_k = \boldsymbol{z}_k^* e^{j[(\theta_k^{\boldsymbol{u}})^* - (\theta_k^{\boldsymbol{z}})^*]}$. The optimal solutions $\boldsymbol{u}_k^*$ to problem (33) is feasible and optimal as follows:

$$\min_{\{\boldsymbol{u}_k^*\}} \sum_{k=1}^K \|\boldsymbol{u}_k^*\|^2 + \sum_{\ell=1}^L (\widetilde{p}_\ell^H)^2 \tag{52a}$$

$$\text{s.t.} \sqrt{\sum_{i\neq k}^K |\boldsymbol{h}_k^\dagger \boldsymbol{u}_i^*|^2 + \sum_{\ell=1}^L |h_{k,\ell}|^2 (\widetilde{p}_\ell^H)^2 + \bar{\sigma}_k^{\mathrm{M}}} \le \frac{\boldsymbol{h}_k^\dagger \boldsymbol{u}_k^*}{\sqrt{\gamma_k^M}} e^{-j(\theta_k^{\boldsymbol{u}})^*}\ \forall k \tag{52b}$$

$$\sqrt{\sum_{j\neq\ell}^L (\widetilde{p}_j^H)^2 |\boldsymbol{v}_\ell^\dagger \boldsymbol{g}_j|^2 + \sum_{k=1}^K |\boldsymbol{v}_\ell^\dagger \boldsymbol{G}\boldsymbol{u}_k^*|^2 + (\widetilde{\sigma}_\ell^{\mathrm{H}})^2} \le \frac{\widetilde{p}_\ell^H \sqrt{|\widetilde{\boldsymbol{v}}_\ell|^2}}{\sqrt{\gamma_\ell^H}}\ \forall \ell \tag{52c}$$

$$\sqrt{q_k^2 + r_k^2} \le \sqrt{1 + \frac{1}{\gamma_k^M}} \boldsymbol{h}_k^\dagger \boldsymbol{u}_k^* e^{-j(\theta_k^{\boldsymbol{u}})^*}\ \forall k \tag{52d}$$

$$\sqrt{(r_k - \alpha_k)^2 + 4\widetilde{\sigma}_k} \le r_k + \alpha_k\ \forall k \tag{52e}$$

$$\sqrt{(q_k - \beta_k)^2 + 4\sqrt{E_k^M}} \le q_k + \beta_k\ \forall k \tag{52f}$$

$$\sqrt{\alpha_k^2 + \beta_k^2} \le 1,\ r_k \ge 0,\ q_k \ge 0\ \forall k \tag{52g}$$

$$\mathrm{Re}(\boldsymbol{h}_k^\dagger \boldsymbol{u}_k^* e^{-j(\theta_k^{\boldsymbol{u}})^*}) \ge 0,\ \mathrm{Im}(\boldsymbol{h}_k^\dagger \boldsymbol{u}_k^* e^{-j(\theta_k^{\boldsymbol{u}})^*}) = 0\ \forall k \tag{52h}$$

where $\bar{\sigma}_k^{\mathrm{M}} = (\sigma_k^{\mathrm{M}})^2 + r_k^2$ and $\widetilde{\boldsymbol{v}}_\ell = \boldsymbol{v}_\ell^\dagger \boldsymbol{g}_\ell$.

Now, the optimal value of problem (8) is not greater than that of the optimal value of problem (52). Similarly, we also can check the optimal solution $\boldsymbol{z}_k^*$. Then, the optimal solution $\boldsymbol{z}_k^*$ to problem (33) is still feasible and optimal as follows:

$$\min_{\{\boldsymbol{z}_k^*\}} \sum_{k=1}^K \|\boldsymbol{z}_k^*\|^2 + \sum_{\ell=1}^L (\widetilde{p}_\ell^H)^2 \tag{53a}$$

$$\text{s.t.} \sqrt{\sum_{i\neq k}^K |\boldsymbol{h}_k^\dagger \boldsymbol{z}_i^*|^2 + \sum_{\ell=1}^L |h_{k,\ell}|^2 (\widetilde{p}_\ell^H)^2 + \bar{\sigma}_k^{\mathrm{M}}} \le \frac{\boldsymbol{h}_k^\dagger \boldsymbol{z}_k^*}{\sqrt{\gamma_k^M}} e^{-j(\theta_k^{\boldsymbol{z}})^*}\ \forall k \tag{53b}$$

$$\sqrt{\sum_{j\neq\ell}^L (\widetilde{p}_j^H)^2 |\boldsymbol{v}_\ell^\dagger \boldsymbol{g}_j|^2 + \sum_{k=1}^K |\boldsymbol{v}_\ell^\dagger \boldsymbol{G}\boldsymbol{z}_k^*|^2 + (\widetilde{\sigma}_\ell^{\mathrm{H}})^2} \le \frac{\widetilde{p}_\ell^H \sqrt{|\widetilde{\boldsymbol{v}}_\ell|^2}}{\sqrt{\gamma_\ell^H}}\ \forall \ell \tag{53c}$$

$$\sqrt{q_k^2 + r_k^2} \le \sqrt{1 + \frac{1}{\gamma_k^M}} \boldsymbol{h}_k^\dagger \boldsymbol{z}_k^* e^{-j(\theta_k^{\boldsymbol{z}})^*}\ \forall k \tag{53d}$$

$$\sqrt{(r_k - \alpha_k)^2 + 4\widetilde{\sigma}_k} \le r_k + \alpha_k\ \forall k \tag{53e}$$

$$\sqrt{(q_k - \beta_k)^2 + 4\sqrt{E_k^M}} \le q_k + \beta_k\ \forall k \tag{53f}$$

$$\sqrt{\alpha_k^2 + \beta_k^2} \le 1,\ r_k \ge 0,\ q_k \ge 0\ \forall k \tag{53g}$$

$$\mathrm{Re}(\boldsymbol{h}_k^\dagger \boldsymbol{z}_k^* e^{-j(\theta_k^{\boldsymbol{z}})^*}) \ge 0,\ \mathrm{Im}(\boldsymbol{h}_k^\dagger \boldsymbol{z}_k^* e^{-j(\theta_k^{\boldsymbol{z}})^*}) = 0\ \forall k. \tag{53h}$$

Therefore, we have $\sum_{k=1}^K \|\boldsymbol{u}_k^*\|^2 = \sum_{k=1}^K \|\boldsymbol{z}_k^*\|^2$. It is observed that $\boldsymbol{z}_k^* e^{j[(\theta_k^{\boldsymbol{u}})^* - (\theta_k^{\boldsymbol{z}})^*]}$ is an optimal solution to problem (52), i.e., $\boldsymbol{u}_k^* = \boldsymbol{z}_k^* e^{j[(\theta_k^{\boldsymbol{u}})^* - (\theta_k^{\boldsymbol{z}})^*]} = \boldsymbol{z}_k^*$ $(\forall k \in \mathcal{K})$. Also, $\boldsymbol{u}_k^*$ and $\boldsymbol{z}_k^*$ satisfy the KKT condition of problem (33). Thus, any limit point of Algorithm 2 is also a KKT solution up to phase rotation.

In Algorithm 2, objective function of the problem (8) is nonincreasing $(\sum_{k=1}^K \|\boldsymbol{w}_k\|^2 + \sum_{\ell=1}^L (\widetilde{p}_\ell^H)^2)$. Moreover, Algorithm 2 is alternating by the MMSE solution and SOCP-relaxation convex problem. Therefore, Algorithm 2 has optimality.

REFERENCES

[1] C.-H. Lee, R. Y. Chang, C.-T. Lin, and S.-M. Cheng, "Beamforming and power allocation in dynamic TDD networks supporting machine-type communication," in *Proc. IEEE Int. Conf. Commun. (ICC)*, Jun. 2020, pp. 1–6.

[2] L. Liu, E. G. Larsson, W. Yu, P. Popovski, C. Stefanovic, and E. de Carvalho, "Sparse signal processing for grant-free massive connectivity: A future paradigm for random access protocols in the Internet of Things," *IEEE Signal Process. Mag.*, vol. 35, no. 5, pp. 88–99, Sep. 2018.

[3] N. Xia, H.-H. Chen, and C.-S. Yang, "Radio resource management in machine-to-machine communications—A survey," *IEEE Commun. Surveys Tuts.*, vol. 20, no. 1, pp. 791–828, 1st Quart., 2018.

[4] A. Aijaz, M. Tshangini, M. R. Nakhai, X. Chu, and A.-H. Aghvami, "Energy-efficient uplink resource allocation in LTE networks with M2M/H2H co-existence under statistical QoS guarantees," *IEEE Trans. Commun.*, vol. 62, no. 7, pp. 2353–2365, Jul. 2014.

[5] N. Abuzainab, W. Saad, C. S. Hong, and H. V. Poor, "Cognitive hierarchy theory for distributed resource allocation in the Internet of Things," *IEEE Trans. Wireless Commun.*, vol. 16, no. 12, pp. 7687–7702, Dec. 2017.

[6] M. K. Elhattab, M. M. Elmesalawy, and I. I. Ibrahim, "A game theoretic framework for device association in heterogeneous cellular networks with H2H/IoT co-existence," *IEEE Commun. Lett.*, vol. 21, no. 2, pp. 362–365, Feb. 2017.

[7] M. K. Elhattab, M. M. Elmesalawy, and I. I. Ibrahim, "Opportunistic device association for heterogeneous cellular networks with H2H/IoT co-existence under QoS guarantee," *IEEE Internet Things J.*, vol. 4, no. 5, pp. 1360–1369, Oct. 2017.

[8] V. Mancuso, P. Castagno, M. Sereno, and M. A. Marsan, "Modeling MTC and HTC radio access in a sliced 5G base station," *IEEE Trans. Netw. Service Manag.*, vol. 18, no. 2, pp. 2208–2225, Jan. 2021.

[9] X. Kuai, X. Yuan, W. Yan, and Y.-C. Liang, "Coexistence of human-type and machine-type communications in uplink massive MIMO," *IEEE J. Sel. Areas Commun.*, vol. 39, no. 3, pp. 804–819, Mar. 2021.

[10] N. Alhussien and T. A. Gulliver, "Optimal resource allocation in cellular networks with H2H/M2M coexistence," *IEEE Trans. Veh. Technol.*, vol. 69, no. 11, pp. 12951–12962, Nov. 2020.

[11] A. Höglund *et al.*, "Overview of 3GPP release 14 enhanced NB-IoT," *IEEE Netw.*, vol. 31, no. 6, pp. 16–22, Nov./Dec. 2017.

[12] P. Kamalinejad, C. Mahapatra, Z. Sheng, S. Mirabbasi, V. C. M. Leung, and Y. L. Guan, "Wireless energy harvesting for the Internet of Things," *IEEE Commun. Mag.*, vol. 53, no. 6, pp. 102–108, Jun. 2015.

[13] B. Clerckx, H. V. Poor, D. In Kim, D. W. K. Ng, R. Schober, and R. Zhang, "Fundamentals of wireless information and power transfer: From RF energy harvester models to signal and system designs," *IEEE J. Sel. Areas Commun.*, vol. 37, no. 1, pp. 4–33, Jan. 2019.

[14] D. Ma, G. Lan, M. Hassan, W. Hu, and S. K. Das, "Sensing, computing, and communications for energy harvesting IoTs: A survey," *IEEE Commun. Surveys Tuts.*, vol. 22, no. 2, pp. 1222–1250, 2nd Quart., 2020.

[15] Q. Qi, X. Chen, and D. W. K. Ng, "Robust beamforming for NOMA-based cellular massive IoT with SWIPT," *IEEE Trans. Signal Process.*, vol. 68, pp. 211–224, Jan. 2020.

[16] Y. Hu, Y. Zhu, M. C. Gursoy, and A. Schmeink, "SWIPT-enabled relaying in IoT networks operating with finite blocklength codes," *IEEE J. Sel. Areas Commun.*, vol. 37, no. 1, pp. 74–88, Jan. 2019.

[17] J. Tang, D. K. C. So, N. Zhao, A. Shojaeifard, and K.-K. Wong, "Energy efficiency optimization with SWIPT in MIMO broadcast channels for Internet of Things," *IEEE Internet Things J.*, vol. 5, no. 4, pp. 2605–2619, Aug. 2018.

[18] Z. Deng, Q. Li, Q. Zhang, L. Yang, and J. Qin, "Beamforming design for physical layer security in a two-way cognitive radio IoT network with SWIPT," *IEEE Internet Things J.*, vol. 6, no. 6, pp. 10786–10798, Dec. 2019.

[19] D. Mishra, G. C. Alexandropoulos, and S. De, "Energy sustainable IoT with individual QoS constraints through MISO SWIPT multicasting," *IEEE Internet Things J.*, vol. 5, no. 4, pp. 2856–2867, Aug. 2018.

[20] J. Yuan, Q. He, M. Matthaiou, T. Q. S. Quek, and S. Jin, "Toward massive connectivity for IoT in mixed-ADC distributed massive MIMO," *IEEE Internet Things J.*, vol. 7, no. 3, pp. 1841–1856, Mar. 2020.

[21] S. K. Nobar, M. H. Ahmed, Y. Morgan, and S. A. Mahmoud, "Uplink resource allocation in energy harvesting cellular network with H2H/M2M coexistence," *IEEE Trans. Wireless Commun.*, vol. 19, no. 8, pp. 5101–5116, Aug. 2020.

[22] "Technical specification group radio access network; Further enhancements to LTE TDD for DL-UL interference management and traffic adaptation (release 11), v11.0.0," 3GPP, Sophia Antipolis, France, Rep. TR 36.828, Jun. 2012.

[23] Z. Shen, A. Khoryaev, E. Eriksson, and X. Pan, "Dynamic uplink-downlink configuration and interference management in TD-LTE," *IEEE Commun. Mag.*, vol. 50, no. 11, pp. 51–59, Nov. 2012.

[24] H. Kim, J. Kim, and D. Hong, "Dynamic TDD systems for 5G and beyond: A survey of cross-link interference mitigation," *IEEE Commun. Surveys Tuts.*, vol. 22, no. 4, pp. 2315–2348, 4th Quart., 2020.

[25] Y. Ramamoorthi and A. Kumar, "Dynamic time division duplexing for downlink/uplink decoupled millimeter wave based cellular networks," *IEEE Commun. Lett.*, vol. 23, no. 8, pp. 1441–1445, Aug. 2019.

[26] D. D. Penda, L. Fu, and M. Johansson, "Energy efficient D2D communications in dynamic TDD systems," *IEEE Trans. Commun.*, vol. 65, no. 3, pp. 1260–1273, Mar. 2017.

[27] B. Yu, L. Yang, H. Ishii, and S. Mukherjee, "Dynamic TDD support in macrocell-assisted small cell architecture," *IEEE J. Sel. Areas Commun.*, vol. 33, no. 6, pp. 1201–1213, Jun. 2015.

[28] H. G. Kim and H.-S. Cho, "Interference management using crossed-slot in dynamic time division duplexing systems," *IEEE Access*, vol. 7, pp. 135377–135385, 2019.

[29] P. Jayasinghe, A. Tölli, J. Kaleva, and M. Latva-Aho, "Bi-directional beamformer training for dynamic TDD networks," *IEEE Trans. Signal Process.*, vol. 66, no. 23, pp. 6252–6267, Dec. 2018.

[30] E. de O. Cavalcante, G. Fodor, Y. C. B. Silva, and W. C. Freitas, "Bidirectional sum-power minimization beamforming in dynamic TDD MIMO networks," *IEEE Trans. Veh. Technol.*, vol. 68, no. 10, pp. 9988–10002, Oct. 2019.

[31] A. Łukowa and V. Venkatasubramanian, "Centralized UL/DL resource allocation for flexible TDD systems with interference cancellation," *IEEE Trans. Veh. Technol.*, vol. 68, no. 3, pp. 2443–2458, Mar. 2019.

[32] Y. Huang, B. Jalaian, S. Russell, and H. Samani, "Reaping the benefits of dynamic TDD in massive MIMO," *IEEE Systems J.*, vol. 13, no. 1, pp. 117–124, Mar. 2019.

[33] J. Mirza, G. Zheng, K.-K. Wong, and S. Saleem, "Joint beamforming and power optimization for D2D underlaying cellular networks," *IEEE Trans. Veh. Technol.*, vol. 67, no. 9, pp. 8324–8335, Sep. 2018.

[34] Z.-Q. Luo, W.-K. Ma, A. M.-C. So, Y. Ye, and S. Zhang, "Semidefinite relaxation of quadratic optimization problems," *IEEE Signal Process. Mag.*, vol. 27, no. 3, pp. 20–34, May 2010.

[35] M. Grant and S. Boyd. (Jun. 2009). *CVX: MATLAB Software for Disciplined Convex Programming*. [Online]. Available: http://cvxr.com/cvx/

[36] A. B. Gershman, N. D. Sidiropoulos, S. Shahbazpanahi, M. Bengtsson, and B. Ottersten, "Convex optimization based beamforming," *IEEE Signal Process. Mag.*, vol. 27, no. 3, pp. 62–75, May 2010.

[37] A. Wiesel, Y. C. Eldar, and S. Shamai, "Linear precoding via conic optimization for fixed MIMO receivers," *IEEE Trans. Signal Process.*, vol. 54, no. 1, pp. 161–176, Jan. 2006.

[38] Z.-Q. Luo and W. Yu, "An introduction to convex optimization for communications and signal processing," *IEEE J. Sel. Areas Commun.*, vol. 24, no. 8, pp. 1426–1438, Aug. 2006.

[39] C.-H. Lee, T.-H. Chang, and S.-C. Lin, "Transmit-receive beamforming optimization for full-duplex cloud radio access networks," in *Proc. IEEE GLOBECOM*, Dec. 2016, pp. 1–6.

[40] F. Rashid-Farrokhi, K. J. R. Liu, and L. Tassiulas, "Transmit beamforming and power control for cellular wireless systems," *IEEE J. Sel. Areas Commun.*, vol. 16, no. 8, pp. 1437–1450, Oct. 1998.

[41] W. Yu and T. Lan, "Transmitter optimization for the multi-antenna downlink with per-antenna power constraints," *IEEE Trans. Signal Process.*, vol. 55, no. 6, pp. 2646–2660, Jun. 2007.

[42] T.-H. Chang, Y.-F. Liu, and S.-C. Lin, "QoS-based linear transceiver optimization for full-duplex multiuser communications," *IEEE Trans. Signal Process.*, vol. 66, no. 9, pp. 2300–2313, May 2018.

[43] R. Yates, "A framework for uplink power control in cellular radio systems," *IEEE J. Sel. Areas Commun.*, vol. 13, no. 7, pp. 1341–1347, Sep. 1995.

[44] K.-Y. Wang, A. Man-Cho So, T.-H. Chang, W.-K. Ma, and C.-Y. Chi, "Outage constrained robust transmit optimization for multiuser MISO downlinks: Tractable approximations by conic optimization," *IEEE Trans. Signal Process.*, vol. 62, no. 21, pp. 5690–5705, Nov. 2014.

[45] Q. Shi, W. Xu, T.-H. Chang, Y. Wang, and E. Song, "Joint beamforming and power splitting for MISO interference channel with SWIPT: An SOCP relaxation and decentralized algorithm," *IEEE Trans. Signal Process.*, vol. 62, no. 23, pp. 6194–6208, Dec. 2014.

[46] M.-M. Zhao, Q. Shi, Y. Cai, and M.-J. Zhao, "Joint transceiver design for full-duplex cloud radio access networks with SWIPT," *IEEE Trans. Wireless Commun.*, vol. 16, no. 9, pp. 5644–5658, Sep. 2017.

[47] S. Boyd and L. Vandenberghe, *Convex Optimization*. Cambridge, U.K.: Cambridge Univ. Press, 2004.

[48] Q. Shi, M. Razaviyayn, M. Hong, and Z.-Q. Luo, "SINR constrained beamforming for a MIMO multi-user downlink system: Algorithms and convergence analysis," *IEEE Trans. Signal Process.*, vol. 64, no. 11, pp. 2920–2933, Jun. 2016.

[49] S. Goyal, P. Liu, and S. S. Panwar, "User selection and power allocation in full-duplex multicell networks," *IEEE Trans. Veh. Technol.*, vol. 66, no. 3, pp. 2408–2422, Mar. 2017.

[50] S. Luo, R. Zhang, and T. J. Lim, "Downlink and uplink energy minimization through user association and beamforming in C-RAN," *IEEE Trans. Wireless Commun.*, vol. 14, no. 1, pp. 494–508, Jan. 2015.

[51] D. Nguyen, L.-N. Tran, P. Pirinen, and M. Latva-aho, "On the spectral efficiency of full-duplex small cell wireless systems," *IEEE Trans. Wireless Commun.*, vol. 13, no. 9, pp. 4896–4910, Sep. 2014.

[52] C.-H. Lee, R. Y. Chang, C.-T. Lin, and S.-M. Cheng, "Energy-efficient D2D underlaid MIMO cellular networks with energy harvesting," in *Proc. IEEE GLOBECOM*, Dec. 2018, pp. 1–7.

[53] S. K. Sharma and X. Wang, "Toward massive machine type communications in ultra-dense cellular IoT networks: Current issues and machine learning-assisted solutions," *IEEE Commun. Surveys Tuts.*, vol. 22, no. 1, pp. 426–471, 1st Quart. 2020.

[54] G. Gui, M. Liu, F. Tang, N. Kato, and F. Adachi, "6G: Opening new horizons for integration of comfort, security, and intelligence," *IEEE Wireless Commun.*, vol. 27, no. 5, pp. 126–132, Oct. 2020.

[55] H. Huang, Y. Peng, J. Yang, W. Xia, and G. Gui, "Fast beamforming design via deep learning," *IEEE Trans. Veh. Technol.*, vol. 69, no. 1, pp. 1065–1069, Jan. 2020.

Chi-Han Lee (Student Member, IEEE) received the B.S. degree in electronic engineering from Jinwen University of Science and Technology, Taipei, Taiwan, in 2007, and the M.S. degree in electrical engineering from National Chi-Nan University, Nantou, Taiwan, in 2009. He is currently pursuing the Ph.D. degree with the Department of Computer Science and Information Engineering, National Taiwan University of Science and Technology, Taipei.

Since 2017, he has been a Research Assistant with the Research Center for Information Technology Innovation, Academia Sinica, Taipei. His research interests are in signal processing problems in wireless communications, convex optimization, IoT, and their applications.

Mr. Lee has been awarded the 2020 Academia Sinica Travel Grant with U.S.$2K grant for the flagship IEEE International Conference on Communications 2020. He has served as a TPC member for the IEEE ICC Workshop 2020. He is also a Reviewer of the IEEE Internet of Things Journal, ICC, GLOBECOM, PIMRC, and VTC.

Ronald Y. Chang (Senior Member, IEEE) received the B.S. degree in electrical engineering from National Tsing Hua University, Hsinchu, Taiwan, in 2000, the M.S. degree in electronics engineering from National Chiao Tung University, Hsinchu, in 2002, and the Ph.D. degree in electrical engineering from the University of Southern California, Los Angeles, CA, USA, in 2008.

From 2002 to 2003, he was with the Industrial Technology Research Institute, Hsinchu. In 2008, he was a Research Intern with the Mitsubishi Electric Research Laboratories, Cambridge, MA, USA. In 2009, he was involved in the NASA Small Business Innovation Research Projects. Since 2010, he has been with the Research Center for Information Technology Innovation, Academia Sinica, Taipei, Taiwan, where he is currently an Associate Research Fellow (Associate Professor). He was a Visiting Scholar of the Department of Electrical and Computer Engineering, Virginia Tech, Blacksburg, VA, USA, in July–August 2018. His research interests include wireless communications and networking.

Dr. Chang was a recipient of the Best Paper Award from the IEEE Wireless Communications and Networking Conference, in 2012, and the Outstanding Young Scholar Award from the Ministry of Science and Technology, Taiwan, in 2015 and 2017, respectively. He was an Exemplary Reviewer of the IEEE Communications Letters, in 2012, the IEEE Transactions on Communications, in 2015, and the IEEE Transactions on Wireless Communications, in 2017. He currently serves as an Associate Editor for IEEE Access.

Shin-Ming Cheng (Member, IEEE) received the B.S. and Ph.D. degrees in computer science and information engineering from National Taiwan University, Taipei, Taiwan, in 2000 and 2007, respectively.

He was a Postdoctoral Research Fellow with the Graduate Institute of Communication Engineering, National Taiwan University from 2007 to 2012. Since 2012, he has been on the faculty of the Department of Computer Science and Information Engineering, National Taiwan University of Science and Technology, Taipei, where he is currently an Associate Professor. Since 2017, he has been with the Research Center for Information Technology Innovation, Academia Sinica, Taipei, where he is currently a joint Associate Research Fellow. His current research interests are secure mechanism design and security-related platform development in 4G/5G networks and IoT networks. Recently, he is investigating the robustness issue in machine learning.

Dr. Cheng received 2014 K. T. Li Young Researcher Award from ACM Taipei/Taiwan Chapter, IEEE PIMRC 2013 Best Paper Award, and CISC 2020 Best Paper Award.

Chia-Hsiang Lin (Member, IEEE) received the B.S. degree in electrical engineering and the Ph.D. degree in communications engineering from National Tsing Hua University (NTHU), Hsinchu, Taiwan, in 2010 and 2016, respectively.

From 2015 to 2016, he was a visiting student with Virginia Tech, Blacksburg, VA, USA. He is currently an Assistant Professor with the Department of Electrical Engineering, and also with the Miin Wu School of Computing, National Cheng Kung University (NCKU), Tainan, Taiwan. Before joining NCKU, he held research positions with The Chinese University of Hong Kong, Hong Kong in 2014 and 2017, NTHU from 2016 to 2017, and the University of Lisbon (ULisboa), Lisbon, Portugal, from 2017 to 2018. He was an Assistant Professor with National Central University, Taoyuan City, Taiwan, in 2018, and a Visiting Professor with ULisboa in 2019. His research interests include network science, game theory, convex optimization, and blind signal processing.

Dr. Lin received the Prize Paper Award from IEEE Geoscience and Remote Sensing Society (GRS-S), in 2020, the Top Performance Award from ACM Multimedia, in 2020, and The 3rd Place from AIM Real World Super-Resolution Challenge at IEEE International Conference on Computer Vision, in 2019. He received the Einstein Grant Award from Ministry of Science and Technology (MOST), from 2018 to 2023. In 2016, he received the Outstanding Dissertation Award from Chinese Image Processing and Pattern Recognition Society and the Best Dissertation Award from IEEE GRS-S.

Chiu-Han Hsiao (Member, IEEE) received the Ph.D. degree in computer science from the Department of Information Management, National Taiwan University, Taipei, Taiwan, in 2018.

He is currently an Assistant Research Scientist with the Research Center for Information Technology Innovation, Academia Sinica, Taipei. His research interests include resource management of wireless communication (4G/5G), AI, and cloud computing technologies.